Molecular Cell

Article

PRDX6 dictates ferroptosis sensitivity by directing cellular selenium utilization

Graphical abstract

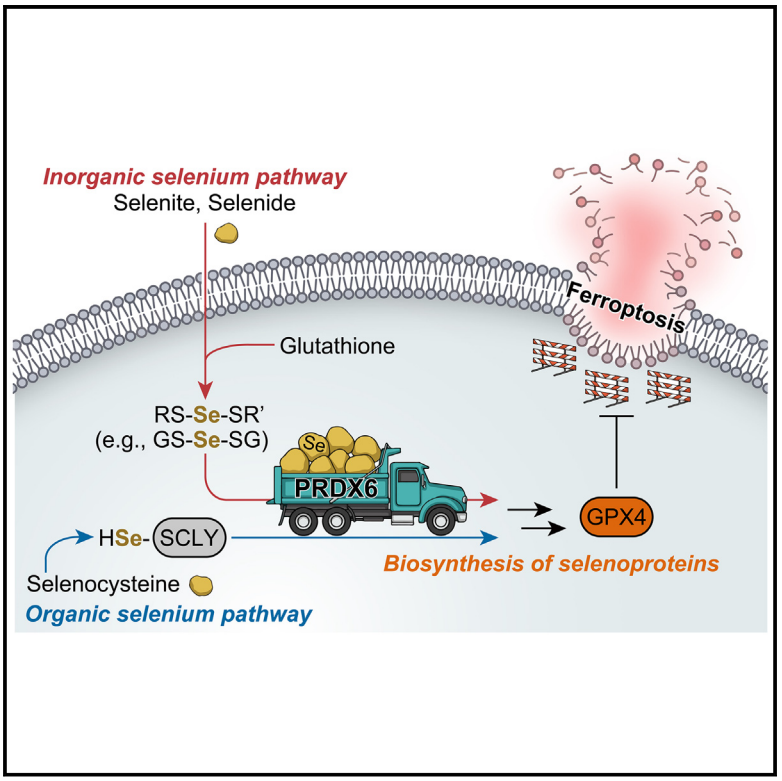

Highlights

- PRDX6 is a key regulator of ferroptosis surveillance
- PRDX6 acts as a selenium acceptor, facilitating selenium utilization
- Selenium covalently binds PRDX6 C47 via GS-Se-SG, serving as a preferred substrate
- PRDX6 deficiency lowers brain GPX4 and raises tumor vulnerability to ferroptosis

Authors

Junya Ito, Toshitaka Nakamura, Takashi Toyama, ..., Kiyotaka Nakagawa, Eikan Mishima, Marcus Conrad

Correspondence

eikan@med.tohoku.ac.jp (E.M.), marcus.conrad@helmholtz-munich.de (M.C.)

In brief

Ito et al. highlight peroxiredoxin 6 (PRDX6) as a critical regulator of ferroptosis. As a selenium-acceptor protein, PRDX6 aids in intracellular selenium utilization for efficient selenoprotein biosynthesis, including glutathione peroxidase 4 (GPX4), the guardian of ferroptosis. PRDX6-deficiency reduces GPX4 expression levels in the mouse brain and increases tumor sensitivity to ferroptosis, underscoring its physiological significance.

Ito et al., 2024, Molecular Cell *84*, 1–16
December 5, 2024
https://doi.org/10.1016/j.molcel.2024.10.028

CellPress

Please cite this article in press as: Ito et al., PRDX6 dictates ferroptosis sensitivity by directing cellular selenium utilization, Molecular Cell (2024), https://doi.org/10.1016/j.molcel.2024.10.028

Molecular Cell

CellPress
OPEN ACCESS

Article

PRDX6 dictates ferroptosis sensitivity by directing cellular selenium utilization

Junya Ito,[1,2] Toshitaka Nakamura,[1] Takashi Toyama,[3] Deng Chen,[1] Carsten Berndt,[4] Gereon Poschmann,[5] André Santos Dias Mourão,[6] Sebastian Doll,[1] Mirai Suzuki,[2] Weijia Zhang,[1] Jiashuo Zheng,[1] Dietrich Trümbach,[1] Naoya Yamada,[1] Koya Ono,[1] Masana Yazaki,[7] Yasutaka Kawai,[7] Mieko Arisawa,[7] Yusuke Ohsaki,[8] Hitoshi Shirakawa,[8] Adam Wahida,[1] Bettina Proneth,[1] Yoshiro Saito,[3] Kiyotaka Nakagawa,[2] Eikan Mishima,[1,9,*] and Marcus Conrad[1,10,*]

[1]Institute of Metabolism and Cell Death, Molecular Targets and Therapeutics Center, Helmholtz Munich, Neuherberg, Bavaria 85764, Germany

[2]Laboratory of Food Function Analysis, Graduate School of Agricultural Science, Tohoku University, Sendai, Miyagi 980-8572, Japan

[3]Laboratory of Molecular Biology and Metabolism, Graduate School of Pharmaceutical Sciences, Tohoku University, Sendai, Miyagi 980-0845, Japan

[4]Department of Neurology, University Hospital and Medical Faculty, Heinrich-Heine University Düsseldorf, Düsseldorf 40225, Germany

[5]Institute of Molecular Medicine, Proteome research, University Hospital and Medical Faculty, Heinrich-Heine University Düsseldorf, Düsseldorf 40225, Germany

[6]Institute of Structural Biology, Helmholtz Zentrum München, Neuherberg, Bavaria 85764, Germany

[7]Department of Bioscience and Biotechnology, Graduate School of Bioresource and Bioenvironmental Sciences, Kyushu University, Fukuoka 819-0395, Japan

[8]Laboratory of Nutrition, Graduate School of Agricultural Science, Tohoku University, Sendai, Miyagi 980-8572, Japan

[9]Division of Nephrology, Rheumatology and Endocrinology, Graduate School of Medicine, Tohoku University, Sendai, Miyagi 980-8574, Japan

[10]Lead contact

*Correspondence: eikan@med.tohoku.ac.jp (E.M.), marcus.conrad@helmholtz-munich.de (M.C.)

https://doi.org/10.1016/j.molcel.2024.10.028

SUMMARY

Selenium-dependent glutathione peroxidase 4 (GPX4) is the guardian of ferroptosis, preventing unrestrained (phospho)lipid peroxidation by reducing phospholipid hydroperoxides (PLOOH). However, the contribution of other phospholipid peroxidases in ferroptosis protection remains unclear. We show that cells lacking GPX4 still exhibit substantial PLOOH-reducing capacity, suggesting a contribution of alternative PLOOH peroxidases. By scrutinizing potential candidates, we found that although overexpression of peroxiredoxin 6 (PRDX6), a thiol-specific antioxidant enzyme with reported PLOOH-reducing activity, failed to prevent ferroptosis, its genetic loss sensitizes cancer cells to ferroptosis. Mechanistically, we uncover that PRDX6, beyond its known peroxidase activity, acts as a selenium-acceptor protein, facilitating intracellular selenium utilization and efficient selenium incorporation into selenoproteins, including GPX4. Its physiological significance was demonstrated by reduced GPX4 expression in *Prdx6*-deficient mouse brains and increased sensitivity to ferroptosis in *PRDX6*-deficient tumor xenografts in mice. Our study highlights PRDX6 as a critical player in directing cellular selenium utilization and dictating ferroptosis sensitivity.

INTRODUCTION

Ferroptosis, a regulated cell death modality hallmarked by unrestrained iron-dependent (phospho)lipid peroxidation,[1] has emerged as an important facet of redox cell biology and a promising target for treating human disease.[2–4] Notably, its potential efficacy against (chemo)therapy-resistant and metastasizing cancers positions ferroptosis as a highly promising target for future therapeutic approaches.[5–7] Consequently, the search for viable therapeutic targets to induce ferroptosis has taken center stage in efforts to combat these therapy-resistant cancers.[8]

Cells have developed various defense systems that detoxify deleterious phospholipid hydroperoxides (PLOOH) to avert ferroptosis.[2,9,10] Among these, selenium-dependent glutathione peroxidase 4 (GPX4) is crucial for preventing ferroptosis by directly reducing PLOOH to their corresponding alcohols at the expense of glutathione (GSH).[11,12] As a member of the selenoprotein family, GPX4 carries selenocysteine (Sec) in its active site, which is critical for enabling full GPX4 enzymatic activity and protection against peroxide-induced, irreversible overoxidation and enzyme inactivation.[13] In addition to the GSH/GPX4 axis, a series of genetic screens have unveiled alternative ferroptosis surveillance systems, such as the NAD(P)H/ferroptosis suppressor

Please cite this article in press as: Ito et al., PRDX6 dictates ferroptosis sensitivity by directing cellular selenium utilization, Molecular Cell (2024), https://doi.org/10.1016/j.molcel.2024.10.028

protein-1 (FSP1)/ubiquinone or vitamin K system,[14–16] di-/tetrahydrobiopterin/GTP cyclohydrolase 1 (GCH1)/dihydrofolate reductase (DHFR) system,[17,18] and 7-dehydrocholesterol reductase (DHCR7),[19–21] which can act as backup systems for GPX4 at least in certain cellular contexts. Unlike GPX4, these systems protect against the lipid peroxidation chain reaction by reducing phospholipid peroxyl radicals that require additional steps for their decomposition.

Akin to GPX4, selenium-independent peroxiredoxin 6 (PRDX6), one of six thiol-specific antioxidant protein family members, has been reported to directly reduce PLOOH to their corresponding alcohols.[10,22,23] Interestingly, PRDX6 acts as a bifunctional enzyme with glutathione peroxidase and phospholipase A2 (PLA_2) activity.[24] Its peroxidase activity depends on the catalytic cysteine residue at position 47 and uses the cofactor GSH as the physiological reductant.[25] Earlier work suggested that genetic perturbation of PRDX6 renders cancer cells more vulnerable to ferroptosis.[26–28] In addition, PRDX6 has been repeatedly identified in genetic screens and gene cluster analyses aimed at identifying genes involved in ferroptosis regulation.[18,29] However, the mechanisms by which PRDX6 modulates ferroptosis susceptibility or its impact on PLOOH reduction remain poorly understood.

In this study, we set out to unravel the purported role of PRDX6 in ferroptosis regulation by preventing uncontrolled (phospho) lipid peroxidation. Contrary to our expectations, the role of PRDX6 in determining ferroptosis sensitivity was not related to intracellular PLOOH reduction or its PLA_2 activity but rather to its crucial involvement in the biosynthesis of selenoproteins, including GPX4, by acting as a selenium-acceptor protein. These findings underscore PRDX6 as a pivotal player participating in intracellular selenium utilization, thereby closing a gap in our understanding of how PRDX6 impacts cellular susceptibility to ferroptosis.

RESULTS

PCOOH reduction capacity is preserved in GPX4-deficient cells

To assess the exact contribution of GPX4 in PLOOH reduction, we established a mass-spectrometry-based method to evaluate the extent of PLOOH reduction using cell lysate samples (Figure 1A).[30] Hereby, synthesized deuterium-labeled phosphatidylcholine hydroperoxide (PCOOH-d_9; prepared as shown in Figure S1) was incubated with enzymes or cell lysates for 1 h, after which the extent of PCOOH reduction was evaluated using liquid chromatography-tandem mass spectrometry (LC-MS/MS). Affinity-purified GPX4 collected from cells overexpressing Strep-II-tagged human GPX4 efficiently reduced labeled PCOOH in a dose-dependent manner (Figure 1B), validating this assay for accessing the PCOOH-reducing activity of the enzymes including GPX4. When PCOOH was incubated with cell lysates collected from human fibrosarcoma HT-1080 cells, a cell line frequently used in ferroptosis research due to its high susceptibility to ferroptosis, PCOOH was efficiently reduced (~70% reduction) (Figure 1C). To evaluate the impact of GPX4 in PCOOH-reducing activity in cell lysate, we prepared *GPX4* knockout (KO) HT-1080 cells (Figure S2A). Cell lysates collected from *GPX4* KO HT-1080 cells showed a significant decrease in PCOOH-reducing ability by ~10% compared with wild-type (WT) lysates, which was recovered by overexpression of GPX4 (Figure 1C). However, interestingly, PCOOH-reducing activity was still preserved in the *GPX4* KO cells (~65% PCOOH reduction). This residual PCOOH-reducing ability in the lysate collected from GPX4-deficient cells was also confirmed in Pfa1 cells, widely used mouse embryonic fibroblasts in ferroptosis research, where treatment with 4-hydroxytamoxifen (TAM) induces *Gpx4* deletion and ferroptosis[31] (Figure S2B).

In line with these *in vitro* findings, although hepatocyte-specific *Gpx4* KO mice maintained on a low-vitamin-E diet exhibits overt ferroptotic cell death in hepatocytes,[14] PCOOH levels in the liver were not significantly different between control and *Gpx4* KO liver samples (although with the limitation of the small sample numbers) (Figure S2C). These findings suggest that GPX4 may not be the prime enzyme responsible for overall cellular PCOOH reduction and imply the presence of an alternative and GPX4-independent PCOOH-reducing pathway(s). Indeed, PCOOH-reducing capacity was lost in the heated cell lysate collected from HT-1080 cells and cells overexpressing GPX4 (Figure S2D), suggesting that other reductase(s) or molecule(s) that are sensitive to heat are responsible for GPX4-independent PCOOH reduction. Consequently, we shifted our focus to PRDX6, a putative alternative enzyme with reported PLOOH-reducing activity.[22,23]

Overexpression of PRDX6 fails to protect against ferroptosis

Next, we explored the PCOOH-reductive capacity of PRDX6 using our established PCOOH-d_9 and LS-MS/MS method. Recombinant PRDX6 exhibited PCOOH-reducing activity; however, its activity was much lower than that of GPX4 in this assay (Figure 1D). Although GPX4 completely reduced PCOOH at 45 nM, PRDX6 reduced only about 60% of PCOOH even at 300 μM. Additionally, cell lysates collected from *PRDX6* KO HT-1080 cells also exhibited PCOOH-reducing capacity (Figures 1E and S2E). Furthermore, cell lysates collected from *PRDX6* KO cells and hPRDX6-reconstituted cells showed comparable PCOOH reduction capacity, suggesting that PRDX6 does not primarily contribute to overall cellular PCOOH reduction. Moreover, in contrast to the overexpression of other ferroptosis suppressors, such as FSP1 and GCH1,[15,17] which effectively prevented ferroptosis induced by TAM-induced *Gpx4* deletion in Pfa1 cells, overexpression of mouse PRDX6 did not protect cells against ferroptosis (Figure 1F). Similarly, human PRDX6 (hPRDX6) showed no ferroptosis-protective effect when overexpressed, regardless of the presence or absence of a tag sequence (Figure S2F). Hence, we concluded that overexpression of PRDX6, unlike GPX4, does not significantly increase the cellular PCOOH-reducing capacity nor prevent ferroptosis.

PRDX6 deletion decreases GPX4 expression and sensitizes cancer cells to ferroptosis

To further investigate the potential role of PRDX6 in ferroptosis regulation, we examined its impact on GPX4 expression. Remarkably, deletion of PRDX6 considerably decreased GPX4 protein expression in HT-1080 cells (Figure 2A), in contrast to

Please cite this article in press as: Ito et al., PRDX6 dictates ferroptosis sensitivity by directing cellular selenium utilization, Molecular Cell (2024), https://doi.org/10.1016/j.molcel.2024.10.028

CellPress
OPEN ACCESS

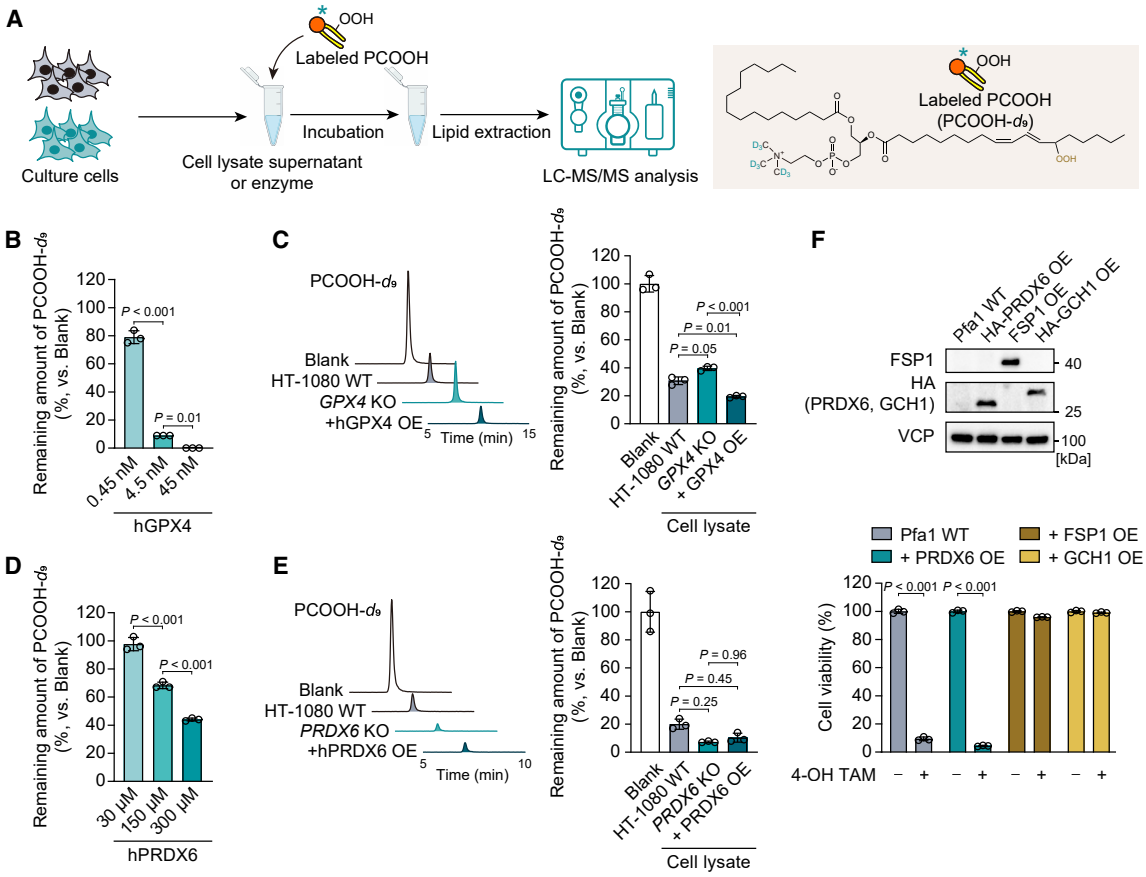

Figure 1. PCOOH-reducing capacity in cells lacking either GPX4 or PRDX6

(A) Scheme for the assessment of PCOOH-reducing capacity. After the incubation of deuterium-labeled phosphatidylcholine hydroperoxide (PCOOH-d_9) with enzymes or cell lysate supernatants, the remaining amount of PCOOH-d_9 was analyzed by LC-MS/MS.

(B) PCOOH-reducing capacity of affinity-purified human GPX4 (0.45, 4.5, and 45 nM). After incubation of PCOOH-d_9, with GPX4 and GSH for 60 min at 37°C, the remaining level of PCOOH-d_9 was determined.

(C) PCOOH-reducing capacity using cell lysates collected from wild-type (WT), *GPX4* knockout (KO) HT1080 cells, and *GPX4* KO cells with OE of hGPX4. The chromatogram (left) and relative value of the remaining PCOOH-d_9 (right) are shown.

(D) PCOOH-reducing capacity of recombinant human PRDX6 (30, 150, and 300 μM).

(E) PCOOH-reducing capacity using cell lysate collected from WT, *PRDX6* KO, and *PRDX6* KO HT1080 cells overexpressing of hPRDX6.

(F) Cell viability of Pfa1 cells stably overexpressing HA-tagged mPRDX6, hFSP1, or HA-hGCH1. Viability was measured 72 h after 4-hydroxytamoxifen (TAM) treatment to deplete *Gpx4*. Immunoblotting analysis showing overexpression of PRDX6, FSP1, or GCH1. Valosin-containing protein (VCP) was used as a loading control. Data are mean ± SD of $n = 3$ (B)–(F). ANOVA, Tukey (B)–(F).

the deletion of any of the other PRDX family members (PRDX1-5)[32] (Figure 2B). The decreased expression of GPX4 in *PRDX6* KO cells was also observed in various cancer cell lines (Figure 2C). Supporting our results, a significant correlation was found between PRDX6 and GPX4 protein expression across a comprehensive proteomic dataset (www.depmap.org) containing 375 cancer cell lines (Figure 2D).

To ascertain the functional consequences, we evaluated ferroptosis susceptibility in cells lacking *PRDX6*. *PRDX6* KO HT-1080 cells exhibited increased sensitivity to ferroptosis compared with WT cells when treated with a wide array of ferroptosis inducers and sensitizers,[33] such as the widely used inhibitor of GPX4 (*1S,3R*)-RSL (RSL3),[12,30] the cystine/glutamate antiporter (xCT) inhibitor erastin,[1] the GSH biosynthesis inhibitor buthionine sulfoximine (BSO), and several FSP1 inhibitors (iFSP1,[15] viFSP1,[34] and icFSP1[35]) (Figure 2E). The increased sensitivity to ferroptosis in *PRDX6* KO HT-1080 cells was entirely restored by the ferroptosis inhibitor liproxstatin-1 (Lip-1).[11] Additionally, *PRDX6* KO consistently increased sensitivity to ferroptosis induced by RSL3 and erastin in various cancer cell lines (Figure 2F). However, the effect of *PRDX6* KO on increasing the cell's sensitivity to RSL3 was not significant in H460 human cancer cells because GPX4 is not essential for their survival.[16,35] These results underscore the important role of PRDX6 in modulating GPX4 expression and thereby regulating cells' susceptibility to ferroptosis.

PRDX6 is involved in intracellular selenium metabolism

To systematically explore the contribution of PRDX6 to GPX4 expression, we sought to identify genetic co-dependencies

Please cite this article in press as: Ito et al., PRDX6 dictates ferroptosis sensitivity by directing cellular selenium utilization, Molecular Cell (2024), https://doi.org/10.1016/j.molcel.2024.10.028

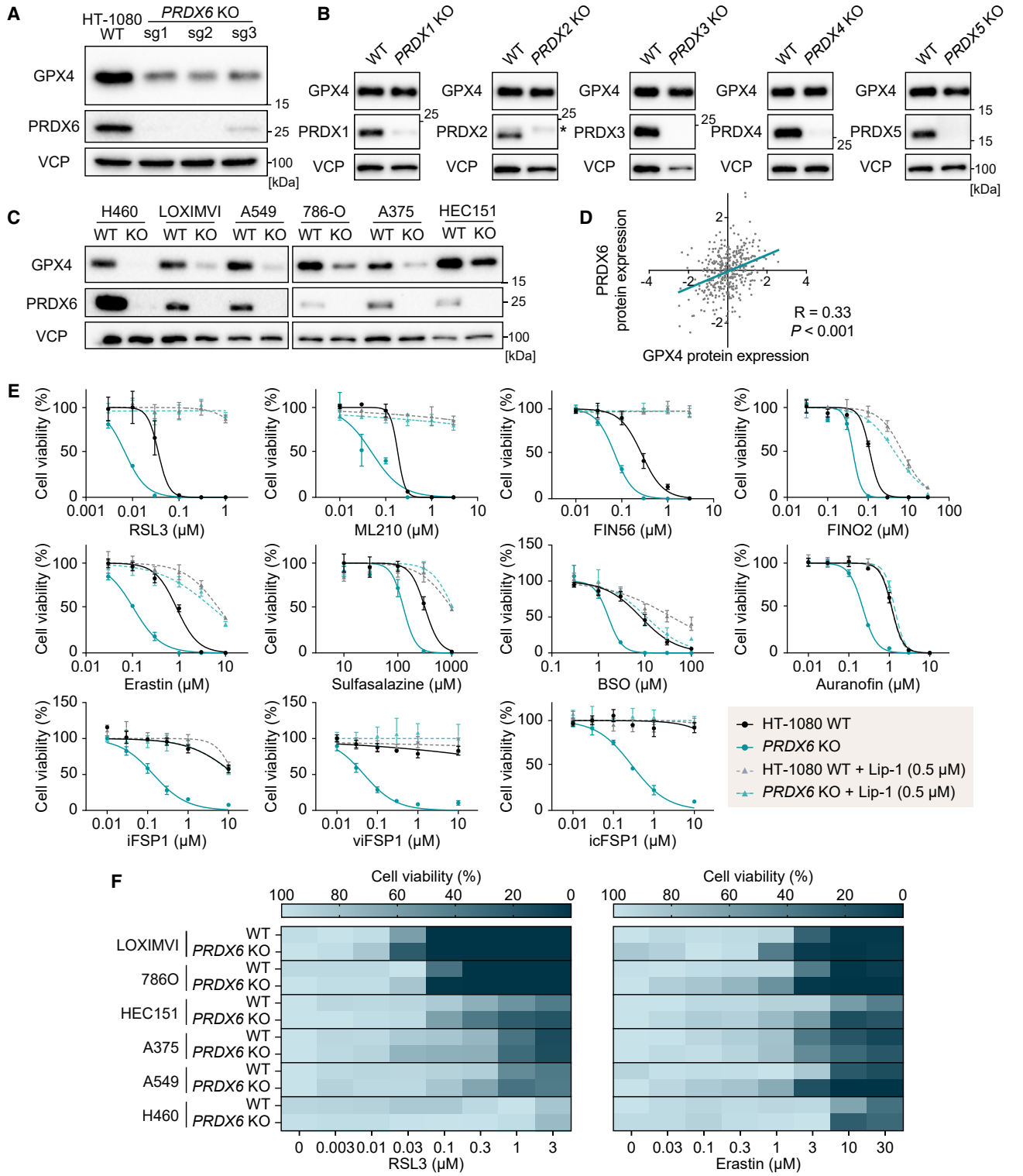

Figure 2. Deletion of *PRDX6* decreases GPX4 protein expression and sensitizes cells to ferroptosis

(A) Immunoblot analysis of GPX4 and PRDX6 in WT and *PRDX6* knockout KO HT-1080 cells.

(B) Immunoblot analysis of GPX4 and PRDX1-5 in WT and *PRDX1-5* KO HT-1080 cells. For the PRDX2 immunoblot, the asterisk indicates a non-specific band.

(C) Immunoblot analysis of WT and *PRDX6* KO NCI-H460, LOXIMVI, A549, 786-O, A375, and HEC151 cells.

(D) Correlation of GPX4 and PRDX6 expression across various cancer cell lines in the proteomics dataset (depmap; version v23Q4).

(legend continued on next page)

Please cite this article in press as: Ito et al., PRDX6 dictates ferroptosis sensitivity by directing cellular selenium utilization, Molecular Cell (2024), https://doi.org/10.1016/j.molcel.2024.10.028

using the depmap CRISPR screen database[36] (Figure 3A). Among the top *PRDX6*-correlated genes, we found several genes crucial for the selenium metabolism pathway, such as LDL-receptor-related protein 8 (*LRP8*; aka apolipoprotein E receptor 2, *APOER2*), selenophosphate synthetase 2 *(SEPHS2)*, O-phosphoseryl-tRNA(Sec) selenium transferase (*SEPSECS*), and selenocysteine lyase (*SCLY*), alongside with genes involved in glutathione metabolism, such as glutathione synthetase (*GSS*), gamma-glutamylcysteine ligase, catalytic subunit (*GCLC*) and gamma-glutamylcysteine ligase, modifier subunit (*GCLM*), and the cognate ferroptosis suppressor apoptosis-inducing factor mitochondria-associated 2 (*AIFM2*), encoding FSP1 (Figure 3A). Supporting this notion, a gene cluster analysis of coessentiality correlation network data[37] indicated a close relationship between *PRDX6* with other genes involved in selenium metabolism and selenoproteins, including *GPX4* (Figure 3B) as previously reported.[29] A correlation of expression levels between PRDX6 and genes associated with selenium metabolism pathway and other selenoproteins was also observed in the depmap proteomics dataset (Figure S3). These correlations strongly suggest that PRDX6 may regulate GPX4 expression through selenium metabolism.

Next, we found that *PRDX6* KO does not alter *GPX4* mRNA levels (Figure 3C), suggesting that the impact of PRDX6 deletion on decreased GPX4 expression occurs at the translational level rather than at the transcriptional level. Because co-translational Sec incorporation at the UGA opal codon is the rate-limiting step in GPX4 translation,[29,38] we examined the effect of selenium supplementation on the decreased level of GPX4 in *PRDX6* KO cells. When L-selenocystine (the dimeric and oxidized form of L-selenocysteine; Sec2) or sodium selenite (Na_2SeO_3) were supplemented into the culture medium as selenium sources, the expression of GPX4 increased in a dose-dependent manner, starting at a 10-nM dose of each selenium source in *PRDX6* KO cells to the same extent as in WT cells (Figure 3D). Supplementation of selenomethionine, an organic form of selenium, also increased GPX4 expression in *PRDX6* KO cells (Figure S4A). Additionally, selenium supplementation rescued the increased susceptibility to ferroptosis observed in *PRDX6* KO cells (Figure 3E). These findings indicate that selenium supplementation can counteract the decrease in GPX4 expression and the resulting increase in ferroptosis vulnerability caused by the loss of *PRDX6*.

To further investigate the emerging relationship between selenium, PRDX6, and GPX4, we examined the effects of selenium deficiency. When cells were cultured in selenium-deficient media for 48 h, GPX4 expression was decreased in WT cells, with almost no GPX4 expression detectable in *PRDX6* KO cells (Figure 3F). A similar tendency was found for glutathione peroxidase 1 (GPX1), another selenoprotein family member known to swiftly react to changing selenium availability.[39] The reduction in GPX4 and GPX1 expression due to selenium deficiency was entirely restored by the supplementation of cells with L-selenocystine or sodium selenite (Figure 3F). Although WT HT-1080 cells remained viable under selenium-deficient conditions, *PRDX6* KO cells exhibited strongly decreased viability, which was entirely restored by Lip-1 and selenium supplementation, as well as reconstitution of PRDX6 expression, demonstrating that selenium deprivation triggered ferroptosis in *PRDX6* KO cells (Figure 3G). This selenium-deprivation-induced cell death in *PRDX6* KO cells began to be induced within several hours after replacing the standard medium with selenium-deficient medium (Figure 3H and Video S1). Consistently, staining of cells with the lipid peroxidation dye C11-BODIPY 581/591 showed that selenium deprivation increased lipid peroxidation in *PRDX6* KO cells in a similar time frame (Figure 3I). These results indicate that PRDX6 is involved in selenium metabolism and regulation of selenoprotein expression, including GPX4. Supporting this notion, the expression levels of other selenoproteins, such as SELENOT, SELENOS, and SEPHS2, were also lower in *PRDX6* KO cells compared with WT cells (Figure 3J). By contrast, no significant changes were observed in the expression of other selenoproteins such as TXNRD1 and TXNRD2 in *PRDX6* KO cells (Figure S4B). It has been known that their protein expression levels are not altered even by the complete loss of selenium incorporation into selenoproteins[13] due to the generation of the truncated variant stopped at the UGA codon located only two amino acids before the actual stop codon, which cannot be distinguished from the full-length protein by immunoblotting due to an almost similar molecular weight.[40] Although *PRDX6* KO cells expressed lower levels of selenoproteins that are sensitive to available selenium amount, *PRDX6* KO did not significantly affect total intracellular selenium levels or the uptake of L-selenocystine and sodium selenite supplemented in the media (Figure S4C). This evidence suggests that PRDX6 acts downstream of selenium uptake, possibly by influencing the efficiency of selenium utilization in cells.

Cysteine 47 of PRDX6 is involved in selenium handling

To investigate the molecular basis of selenium metabolism by PRDX6, we focused on its different active sites relevant for its PLA_2 activity (S32),[24] peroxidase activity (C47),[25] and the alternative cysteine residue (C91) (Figure 4A). We performed site-directed mutagenesis on these residues in hPRDX6 and stably expressed these variants in *PRDX6* KO HT-1080 cells. Although the expression of S32A and C91S mutants allowed the restoration of GPX4 and GPX1 expression levels to WT levels, the C47S mutant failed to restore the expression of both GPX4 and GPX1 (Figures 4B and S4D). Accordingly, the increased ferroptosis sensitivity of *PRDX6*-deficient cells to RSL3 and erastin was restored by overexpression of PRDX6 WT, S32A, and C91S mutants but not by the C47S mutant (Figures 4C and 4D).

Next, we cultured the different PRDX6 mutant lines in selenium-deficient media, revealing that only *PRDX6* KO cells and the cells expressing C47S variant succumbed to cell death, which could be rescued by supplementation of L-selenocystine

(E) Viability of WT and *PRDX6* KO HT-1080 cells treated with various ferroptosis inducers and sensitizers. RSL3, ML210, FIN56, FINO2, and auranofin (for 24 h); erastin and sulfasalazine (for 48 h); and BSO, iFSP1, viFSP1, and icFSP1 (for 72 h). Liproxstatin-1 (Lip-1, 0.5 μM) was used as a ferroptosis inhibitor.
(F) Heatmap showing viability of various WT and *PRDX6* KO cancer cells treated with RSL3 (for 24 h) and erastin (for 48 h). Data are representative of three independent experiments. Data are mean ± SD of $n = 3$ (E) and mean of $n = 3$ (F).

Please cite this article in press as: Ito et al., PRDX6 dictates ferroptosis sensitivity by directing cellular selenium utilization, Molecular Cell (2024), https://doi.org/10.1016/j.molcel.2024.10.028

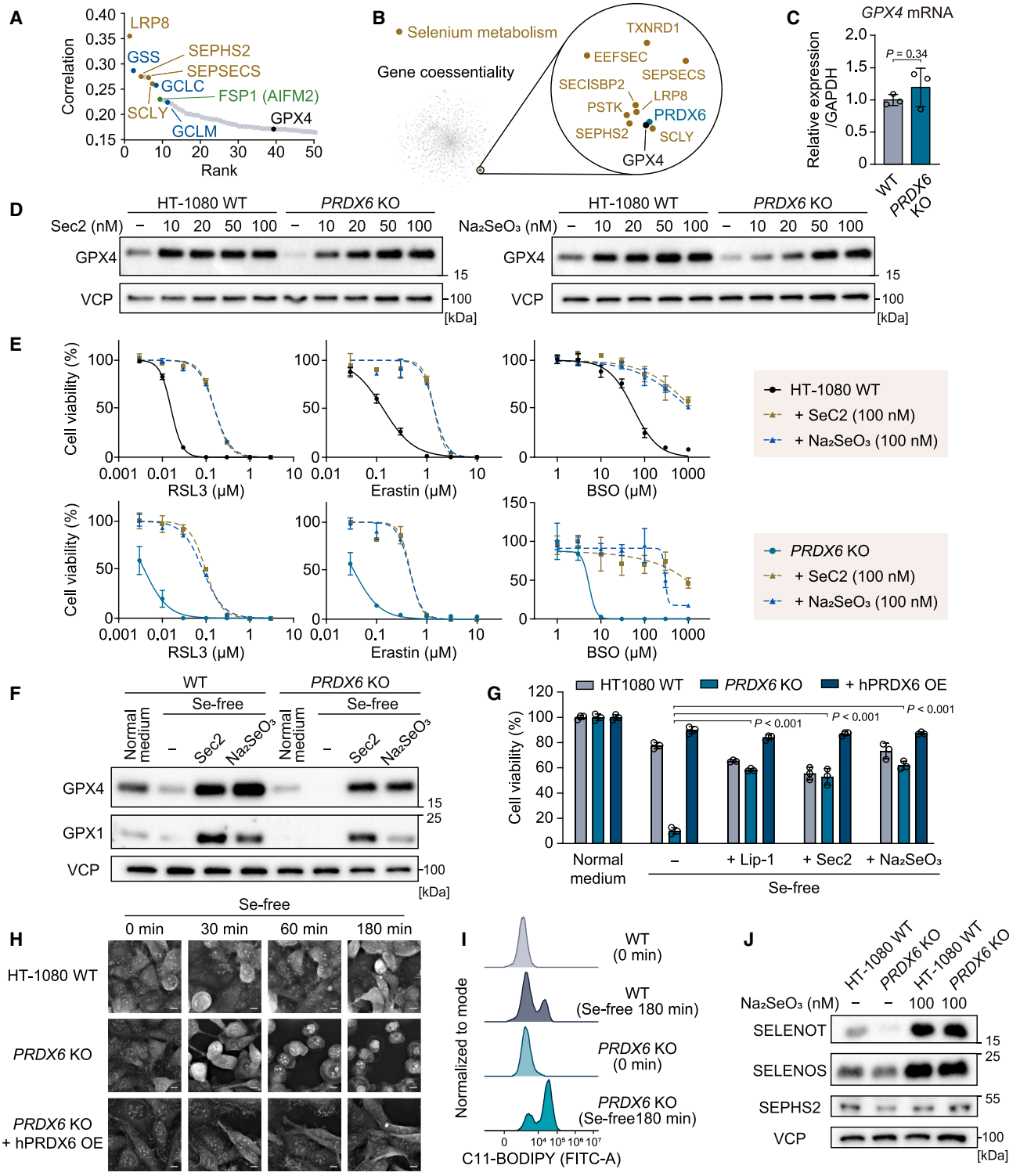

Figure 3. PRDX6 is involved in selenoprotein synthesis and selenium metabolism

(A) Top co-dependent genes with *PRDX6* in depmap CRISPR screen database (https://depmap.org; version v23Q4). Genes related to selenium metabolism (brown), glutathione synthesis (blue), and ferroptosis suppressors (green) are highlighted.

(B) Clustering genes from co-essentiality analysis (http://coessentiality.net). Selenium-metabolism-related cluster is highlighted.

(C) *GPX4* mRNA level in WT and *PRDX6* KO HT-1080 cells.

(legend continued on next page)

Please cite this article in press as: Ito et al., PRDX6 dictates ferroptosis sensitivity by directing cellular selenium utilization, Molecular Cell (2024), https://doi.org/10.1016/j.molcel.2024.10.028

or sodium selenite (Figures 4E and 4F). Treatment with MJ33, an inhibitor of the PLA_2 activity of PRDX6,[41] did not alter the susceptibility of HT1080 WT cells to ferroptosis, supporting that the PLA_2 function is not involved in the regulatory action of PRDX6 in ferroptosis (Figure S4E). These data show that, in the absence of abundant selenium, the peroxidative C47 in PRDX6 is essential for efficient intracellular selenium handling and proper expression of selenoproteins represented by GPX4, thereby protecting cells against ferroptosis.

PRDX6 plays a role in efficient selenium utilization

The general biosynthetic pathway for selenium metabolism for selenoproteins biosynthesis is summarized in Figure 5A.[42] Selenium uptake and intracellular metabolism can be broadly divided into an organic and inorganic pathway. In the organic pathway, the selenium transport protein selenoprotein P (SeP) is taken up by LRP8-mediated endocytosis and degraded in lysosomes, whereupon Sec is released.[29,43] Sec is also supplied by the reduction of selenocystine (the oxidized dimeric form of Sec, Sec2), which is considered to be taken up by xCT (aka. system x_c^-).[44] Subsequently, selenium is released from Sec as a selenide by SCLY[45] or an SCLY-independent pathway.[46] In the inorganic pathway, selenite and its reduced form, selenide, are considered to be transported via different pathways and used as selenium sources.[42] As part of the inorganic pathway, extracellular selenite is converted to its reduced form, selenide, in a step involving xCT,[47,48] which imports extracellular cystine, the oxidized dimeric form of cysteine (note, most cysteine is present in its oxidized form in medium) into cells. After conversion to its reduced form cysteine, it is used for GSH and protein biosynthesis, whereas a fraction is released into the extracellular space.[49,50] This xCT-mediated cystine-cysteine cycle provides extracellular thiol groups to reduce selenite to selenide. Eventually, intracellular selenide derived from both pathways is used as a substrate of SEPHS2 that catalyzes the production of monoselenophosphate, which is then used by SEPSECS to convert O-phosphoseryl-tRNA(Sec) to selenocysteinyl-tRNA(Sec), the latter being used by ribosomes for co-translational incorporation of Sec into selenoproteins.[38]

Our results suggested that PRDX6 is involved in selenium metabolism through its active site at C47, which plays a crucial role in its reducing activity. Therefore, we assessed the involvement of PRDX6 on the expression of GPX4 under cell culture conditions with decreased reducing potential by depleting GSH and/or cysteine because the cysteine/xCT/GSH pathway generates the major cellular reducing capacity.[51] When cellular GSH was depleted by BSO, L-selenocystine and sodium selenite supplementation increased GPX4 expression both in WT and *PRDX6* KO cells. However, *PRDX6* KO cells required a higher amount of selenium (50–100 nM) to afford an increased expression of GPX4 (Figure 5B). A similar finding was observed in cells treated with the xCT inhibitor erastin (Figure S4F). Next, when we cultured the cells in cyst(e)ine-free (Cys-free) media, which decreases both GSH and Cys[52] expression of GPX4, and GPX1 was decreased in WT cells as previously reported[53] and almost absent in *PRDX6* KO cells (Figure 5C). The diminished expression of GPX4 and GPX1 in Cys-free media was rescued by supplementing either with L-selenocystine or sodium selenite in a dose-dependent manner in WT cells, whereas, interestingly, it was rescued in *PRDX6* KO cells by high concentration of L-selenocystine (100 nM) but hardly by sodium selenite supplementation even at concentrations up to 100 nM (Figure 5C). The condition of the Cys-free media was pharmacologically reproduced with inhibitors by cotreatment of the cells with BSO and erastin (Figure 5D). The results showed that the expression of GPX4 and GPX1 in *PRDX6* KO cells was rescued by the addition of L-selenocystine at higher concentrations than required for WT cells, whereas it was hardly increased by sodium selenite supplementation, similar to the result found in Cys-free media. In this condition, in which erastin, BSO, and selenium were added at the same time point, selenium may be utilized already before erastin efficiently inhibits xCT and hence the cellular cyst(e)ine cycle. Thus, we pretreated the cells with erastin and BSO for 24 h before selenium supplementation, under which condition GPX4 and GPX1 levels were hardly recovered by supplementation with either selenium source even at 100 nM (Figure 5E). These results suggest that in the absence of cellular reducing activity by depletion of Cys and GSH, KO of *PRDX6* renders selenite as an almost unusable source. Supporting this notion, treatment with a reducing agent, β-mercaptoethanol, restored decreased GPX4 expression in *PRDX6* KO cells cultured in Cys-free media (Figure 5F). In summary, the results suggest that PRDX6 plays an important role in the efficient selenite utilization in concert with GSH and Cys.

PRDX6 is a selenium-acceptor protein

Based on these findings, we hypothesized that PRDX6 might function as a selenium-acceptor protein required for the effective utilization of selenium in cells. To determine whether PRDX6 directly binds to selenium, we measured PRDX6-selenium adducts using LC-MS (Figures 6A, 6B, and S5A). Our result revealed that the C47 residue of recombinant hPRDX6 forms

(D) Immunoblot analysis of GPX4 in WT and *PRDX6* KO HT-1080 cells treated with indicated concentrations of L-selenocystine (Sec2) or sodium selenite (Na_2SeO_3) for 48 h.
(E) Viability of WT and *PRDX6* KO HT-1080 cells co-treated with ferroptosis inducers (RSL3, erastin, and BSO) and different selenium sources (Sec2 or Na_2SeO_3).
(F) Immunoblot analysis of GPX4 and GPX1 in WT and *PRDX6* KO HT-1080 cells after incubation in selenium-free (Se-free) medium supplemented with Sec2 (100 nM) or Na_2SeO_3 (100 nM) for 48 h.
(G) Viability of WT, *PRDX6* KO, and *PRDX6* KO HT-1080 cells overexpressing hPRDX6 (OE) after incubation in Se-free medium supplemented with Lip-1 (0.5 μM), Sec2 (100 nM), or Na_2SeO_3, (100 nM) for 24 h.
(H) Live imaging of the indicated cells after replacing with Se-free medium. Scale, 10 μm.
(I) C-11 BODIPY 581/591 lipid peroxidation assay of WT and *PRDX6* KO HT-1080 cells before (0 min) and after 180 min-incubation in Se-free media.
(J) Immunoblot analysis of SELENOT, SELENOS, and SEPHS2 in WT and *PRDX6* KO HT-1080 cells treated with or without Na_2SeO_3 for 48 h. Data represent the mean ± SD of $n = 3$ (C); the mean ± SD of three wells from one out of three independent experiments (E) and (G). t test (C) and ANOVA, Tukey (G).

Please cite this article in press as: Ito et al., PRDX6 dictates ferroptosis sensitivity by directing cellular selenium utilization, Molecular Cell (2024), https://doi.org/10.1016/j.molcel.2024.10.028

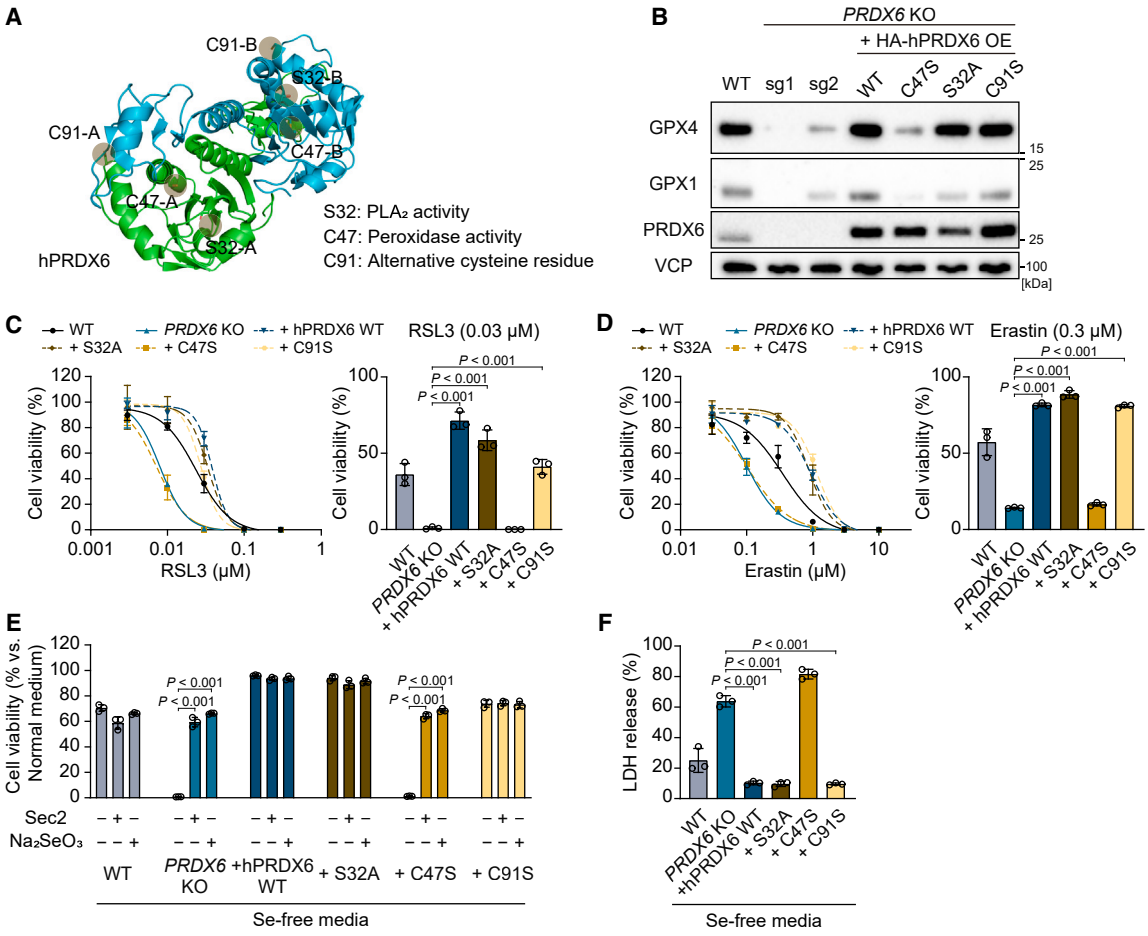

Figure 4. PRDX6 C47 is critical for its role in selenium metabolism

(A) A crystal structure of dimerized hPRDX6 (PDB: 5B6M) highlighting the functional residues studied here.

(B) Immunoblot analysis of WT, *PRDX6* KO (sg1 and sg2), and *PRDX6* KO (sg2) HT-1080 cells overexpressing (OE) each of the different mutants of HA-tagged hPRDX6.

(C and D) Viability of WT, *PRDX6* KO, and *PRDX6* KO HT-1080 cells overexpressing each of the different hPRDX6 mutants treated with RSL3 and erastin for 24 h (left). Data for 30 nM of RSL3 and 0.3 μM of erastin is also shown as a bar graph (right).

(E) Viability of cells 24 h after incubation in Se-free medium supplemented with or without different selenium sources (100 nM of Sec2 or Na_2SeO_3).

(F) LDH release level from the indicated cells cultured in a Se-free medium for 24 h. Data represent the mean ± SD of three wells from one out of three independent experiments (C–F, ANOVA, Tukey).

C47-S-SeH (measured as its carbamidomethyl form) and C47-S-Se-GSH adduct (C47-S-Se-SG). These modifications were only detected when PRDX6 was incubated with selenite and GSH (Figure 6C), suggesting that covalent binding of selenium to PRDX6 depends on the presence of GSH. The analysis also showed selenium binding to C91 residue, which occurred in a similar GSH-dependent manner (Figures S5B and S5C). Furthermore, the selenium binding capacity of PRDX6 was evaluated using inductively coupled plasma-mass spectrometry (ICP-MS), which measures the amount of selenium in samples. The result showed that recombinant WT hPRDX6 binds efficiently to selenium in the presence of GSH, whereas the binding capacity was reduced in the hPRDX6 C47S variant (Figure 6D). Additionally, pre-treatment with the thiol alkylation N-ethylmaleimide (NEM) abrogated the covalent binding of selenium to hPRDX6 WT (Figure S5D). These findings indicate that PRDX6 is a selenium-acceptor protein utilizing its redox-active cysteine residues as binding sites.

Next, we investigated how GSH is involved in selenium binding to PRDX6. GSH is known to react with selenium to form selenodiglutathione (GS-Se-SG).[54] To explore the possibility that GS-Se-SG is a binding substrate for PRDX6, we incubated recombinant hPRDX6 with chemically synthesized GS-Se-SG (Figures 6E and S6). The results showed that selenium in this form efficiently binds to PRDX6, suggesting a model in which PRDX6 covalently binds to selenium in the form of GS-Se-SG. Additionally, the presence of excess GSH in the reaction condition did not significantly decrease the amount of PRDX6-Se binding (Figure 6E), indicating that the formation of PRDX6-Se-SG is chemically equilibrium-dominant in the reaction between PRDX6 and GS-Se-SG (i.e., PRDX6 + GS-Se-SG → PRDX6-S-Se-SG + GSH) (Figure 6F).

Please cite this article in press as: Ito et al., PRDX6 dictates ferroptosis sensitivity by directing cellular selenium utilization, Molecular Cell (2024), https://doi.org/10.1016/j.molcel.2024.10.028

CellPress
OPEN ACCESS

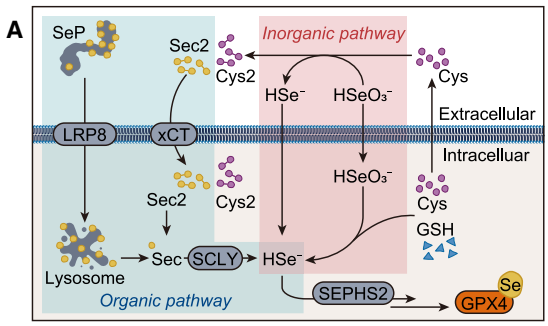

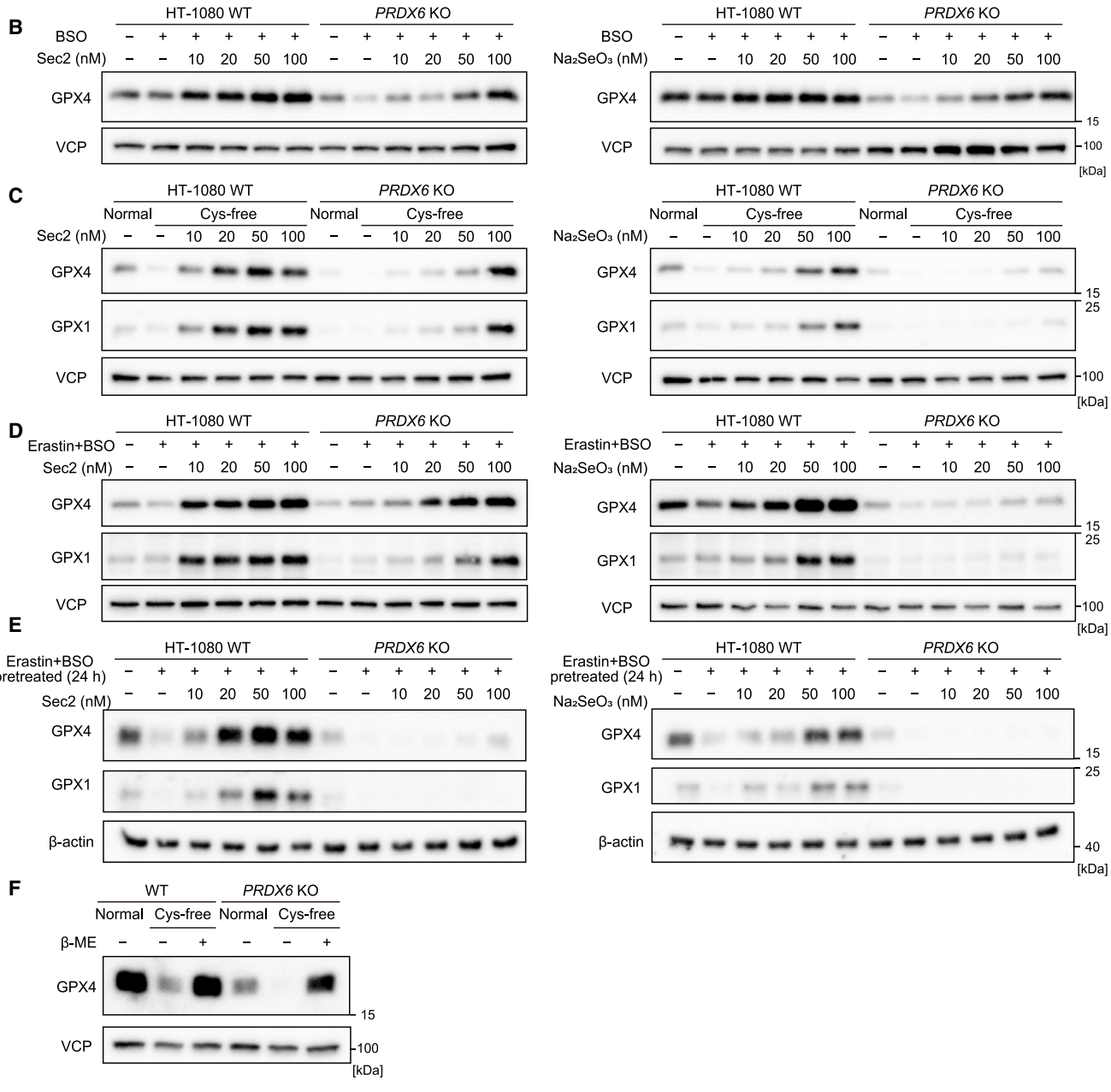

(legend on next page)

Please cite this article in press as: Ito et al., PRDX6 dictates ferroptosis sensitivity by directing cellular selenium utilization, Molecular Cell (2024), https://doi.org/10.1016/j.molcel.2024.10.028

Prdx6-deficient mice exhibit lower selenoprotein expression in brain

To investigate the physiological significance of PRDX6's function in selenium metabolism, we analyzed whole-body *Prdx6*-deficient mice. As previously reported,[55] these mice are viable and do not exhibit overt abnormalities under normal housing conditions with a standard diet, which contains sufficient amounts of selenium (0.5 mg/kg) and vitamin E (60–70 mg/kg). Nonetheless, under these conditions, the expression levels of GPX4 and GPX1 in the brain were found to be markedly lower in *Prdx6* KO mice compared with WT mice (Figure 7A), whereas their expression levels were comparable between the KO and WT mice in the liver and kidney (Figure 7A). These findings demonstrate the crucial role of PRDX6 in selenoprotein expression in certain tissues, such as the brain, even under conditions of sufficient selenium supply *in vivo*.

PRDX6 deficiency suppresses tumor growth synergistically with ferroptosis inducers

To further evaluate the impact of *PRDX6* depletion *in vivo*, we used a xenograft mouse model with subcutaneously implanted WT or *PRDX6* KO human lung cancer A549 cells. BALB/c nude mice implanted with these cells were treated with either vehicle or imidazole-ketone erastin (IKE), a metabolically more stable inhibitor of xCT.[56] The tumor size of *PRDX6* KO cells treated with IKE was significantly smaller than that of WT cells treated with either vehicle or IKE (Figures 7B and 7C). The GPX4 and GPX1 levels were also lower in the tumors derived from *PRDX6* KO cells (Figure 7D, the residual PRDX6 expression in the tumors derived from *PRDX6* KO cells is considered to be from mouse cells (e.g., skin, vessel, and immune cells) contained within the collected tumor tissues). Therefore, the depletion of PRDX6 increased tumor sensitivity to ferroptosis inducers *in vivo*.

DISCUSSION

In this study, we revealed an unexpected moonlighting function of PRDX6 in selenium metabolism. Beyond its known function as a peroxidase and phospholipase, PRDX6 acts as a selenium-acceptor protein, crucial for efficient intracellular selenium utilization. This function facilitates selenium incorporation into selenoproteins, thereby regulating GPX4 expression level and influencing the sensitivity of cells to ferroptosis (Figure 7E).

Our finding highlights the importance of the catalytic residue C47 for selenium utilization, where PRDX6 binds selenium in a GSH-dependent manner, with GS-Se-SG perhaps as a preferred substrate. Given the highly reactive nature of selenide (HSe^-),[57] a reduced form of selenite, and the form providing selenium to SEPHS2, it is postulated that its intracellular trafficking occurs by binding to acceptor molecules and/or proteins,[45] functioning as a "mobile selenium shuttle" within cells. Our findings suggest that PRDX6 is the carrier for selenium utilization in cooperation with GSH and Cys. Based on our finding, a hypothetical model is considered in which the reduced form of PRDX6 reacts with GS-Se-SG, eventually forming PRDX6-C47-S-SeH (Figure 6F). This process may facilitate the efficient metabolism of intracellular selenium and its transfer to SEPHS2, ultimately enabling selenium incorporation into selenoproteins (Figure 7E). Because PRDX6 also influences the expression of selenoproteins beyond GPX4, it is likely to affect the function of these selenoproteins in ways unrelated to ferroptosis suppression. Although the protein levels of TXNRD1 and TXNRD2 were not altered by *PRDX6* KO—potentially due to the presence of truncated forms produced without Sec incorporation—a reduction in the full length, active forms containing Sec would likely impair the redox functions associated with these selenoproteins.

Our results demonstrate that PRDX6-deficient cells require higher concentrations of inorganic selenium (i.e., selenite) and organic selenium, such as L-selenocysteine, compared with WT cells to substantially increase GPX4 levels, especially under conditions with suppressed amounts of GSH in cells. This suggests that PRDX6 plays a role in promoting the efficient utilization of selenium in both the inorganic and organic selenium pathways, involving both SCLY-dependent and -independent mechanisms.[46] These findings align with recent studies by Chen et al. (see companion paper) and Fujita et al.,[58,59] emphasizing the role of PRDX6 as a selenium acceptor.

Previous studies have reported that different cell and tissue types employ distinct selenium uptake/utilization pathways.[46] In addition, selenium content and level can vary between batches of FBS used for cell culture.[43] Therefore, the impact of PRDX6 on selenium utilization and ferroptosis susceptibility may vary depending on the cell type and FBS batches used in cell culture. In the *in vivo* context, the impact of PRDX6 on selenoprotein expression was particularly striking in the brain. Conversely, the lack of a significant difference in GPX4 expression in the liver and kidney is likely due to the high abundance of selenium in these tissues and the fact that selenium uptake into the brain requires a specialized uptake axis.[38] A normal chow diet contains approximately 0.5 mg/kg of selenium, mainly in the forms of selenomethionine and inorganic selenium, which

Figure 5. PRDX6 is involved in cellular selenium utilization

(A) Scheme of the commonly known pathways for cellular selenium uptake and utilization for selenoprotein synthesis. Cys, cysteine; Cys2, cystine; Sec, selenocysteine; Sec2, selenocystine; and SeP, selenoprotein P.

(B) Immunoblot analysis of WT and *PRDX6* KO HT-1080 cells treated with BSO (500 μM), Lip-1 (1 μM), and indicated concentrations of L-selenocystine (Sec2, left) or sodium selenite (Na_2SeO_3, right) for 72 h.

(C) Immunoblot analysis of WT and *PRDX6* KO HT-1080 cells after incubation in cyst(e)ine (Cys)-free media supplemented with 10% dialyzed FBS, Lip-1 (1 μM), and indicated concentrations of Sec2 or Na_2SeO_3 for 72 h.

(D) Immunoblot analysis of WT and *PRDX6* KO HT-1080 cells treated with erastin (10 μM), BSO (500 μM), Lip-1 (1 μM), and indicated concentrations of Sec2 or Na_2SeO_3 for 48 h.

(E) Immunoblot analysis of WT and *PRDX6* KO HT-1080 cells pretreated with erastin (10 μM), BSO (500 μM), and Lip-1 (1 μM) for 24 h, followed by Sec2 or Na_2SeO_3 for 48 h.

(F) Immunoblot analysis of WT and *PRDX6* KO HT-1080 cells treated with Cys-free media with or without β-mercaptoethanol (β-ME, 50 μM) for 48 h.

Please cite this article in press as: Ito et al., PRDX6 dictates ferroptosis sensitivity by directing cellular selenium utilization, Molecular Cell (2024), https://doi.org/10.1016/j.molcel.2024.10.028

CellPress
OPEN ACCESS

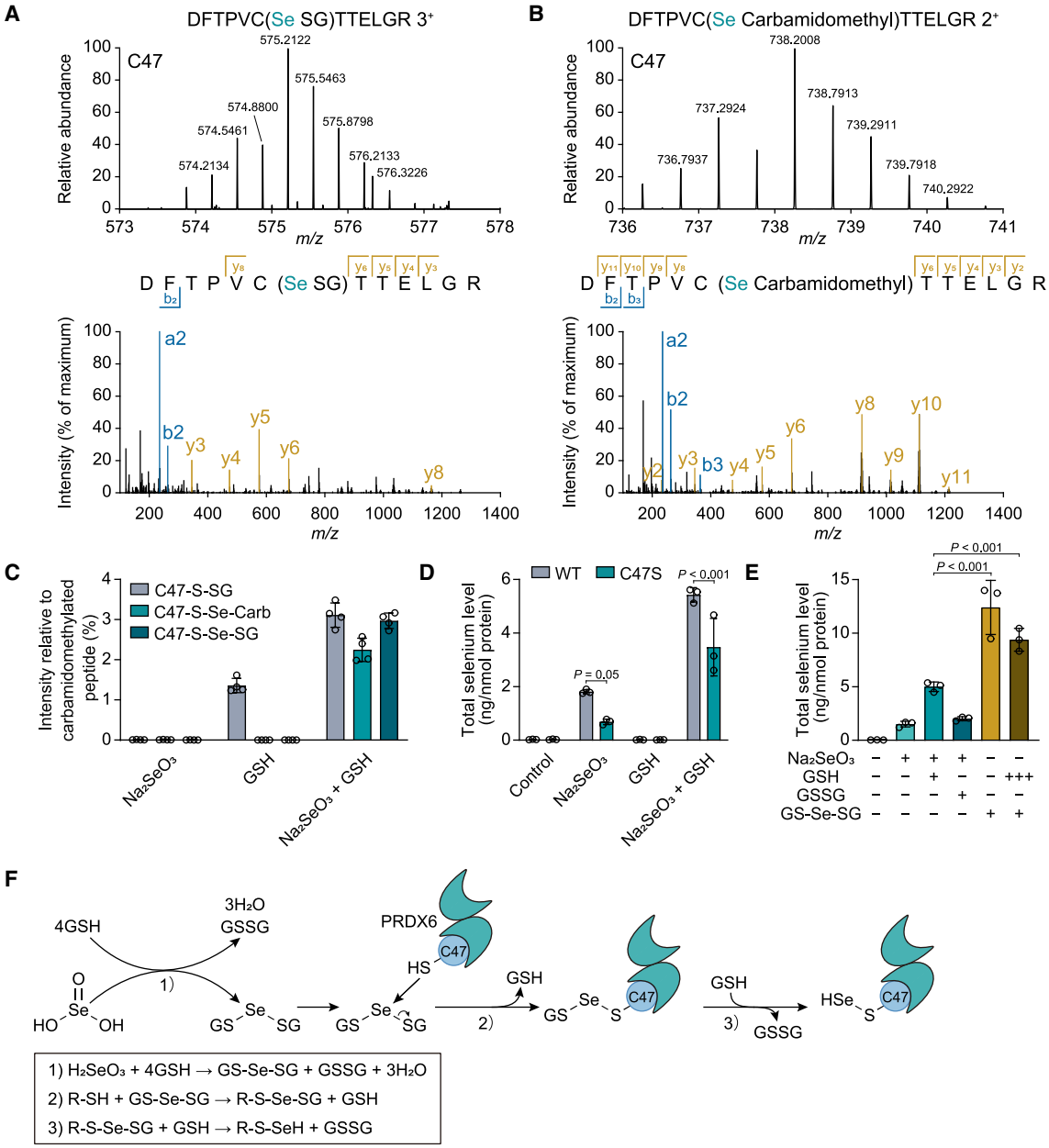

Figure 6. PRDX6 binds to selenium in a GSH-dependent manner

(A and B) Isotopic patterns of precursor mass and corresponding fragment spectra of the C47 residue-containing tryptic peptide of recombinant hPRDX6, including selenium-glutathione (GSH), adduct (Se-SG, A), and carbamidomethylated selenium adduct (Se-Carb, B).

(C) Relative intensity ratio (%) of C47 modification of recombinant hPRDX6 incubated with glutathione (GSH), sodium selenite, and both, measured by LC-MS.

(D) Selenium level bound to recombinant hPRDX6 WT or C47S (40 μM) treated with sodium selenide (Na_2SeO_3, 40 μM), GSH (160 μM), or both. The total selenium content was measured by ICP-MS (D and E).

(E) Selenium level bound to recombinant hPRDX6 WT (40 μM) treated with Na_2SeO_3 (40 μM) + GSH (160 μM) or oxidized glutathione (GSSG, 80 μM), selenodiglutathione (GS-Se-SG, 40 μM) alone, or Gs-Se-Se (40 μM) + excess GSH (1.6 mM).

(F) A hypothetical reaction model for the reduced form of PRDX6 with GS-Se-SG. Mean ± SD of $n = 4$ (C), $n = 3$ (D and E) in each group. ANOVA, Tukey (D and E).

is a sufficient amount to maintain maximal expression levels of selenoproteins in the liver of WT mouse.[60,61] By contrast, selenium supply and utilization are thought to be limited in the brain, which needs to cross the blood-brain barrier. Therefore, PRDX6 is presumed to be more critical for maintaining selenoprotein expression in the brain. This finding is supported by the fact that, although *SELENOP* (encoding SeP) deficient mice can survive on a normal chow diet, they exhibit neurological dysfunction due to low-selenium levels in the brain, particularly when fed a low-selenium diet.[62,63] In addition, the decreased expression

Please cite this article in press as: Ito et al., PRDX6 dictates ferroptosis sensitivity by directing cellular selenium utilization, Molecular Cell (2024), https://doi.org/10.1016/j.molcel.2024.10.028

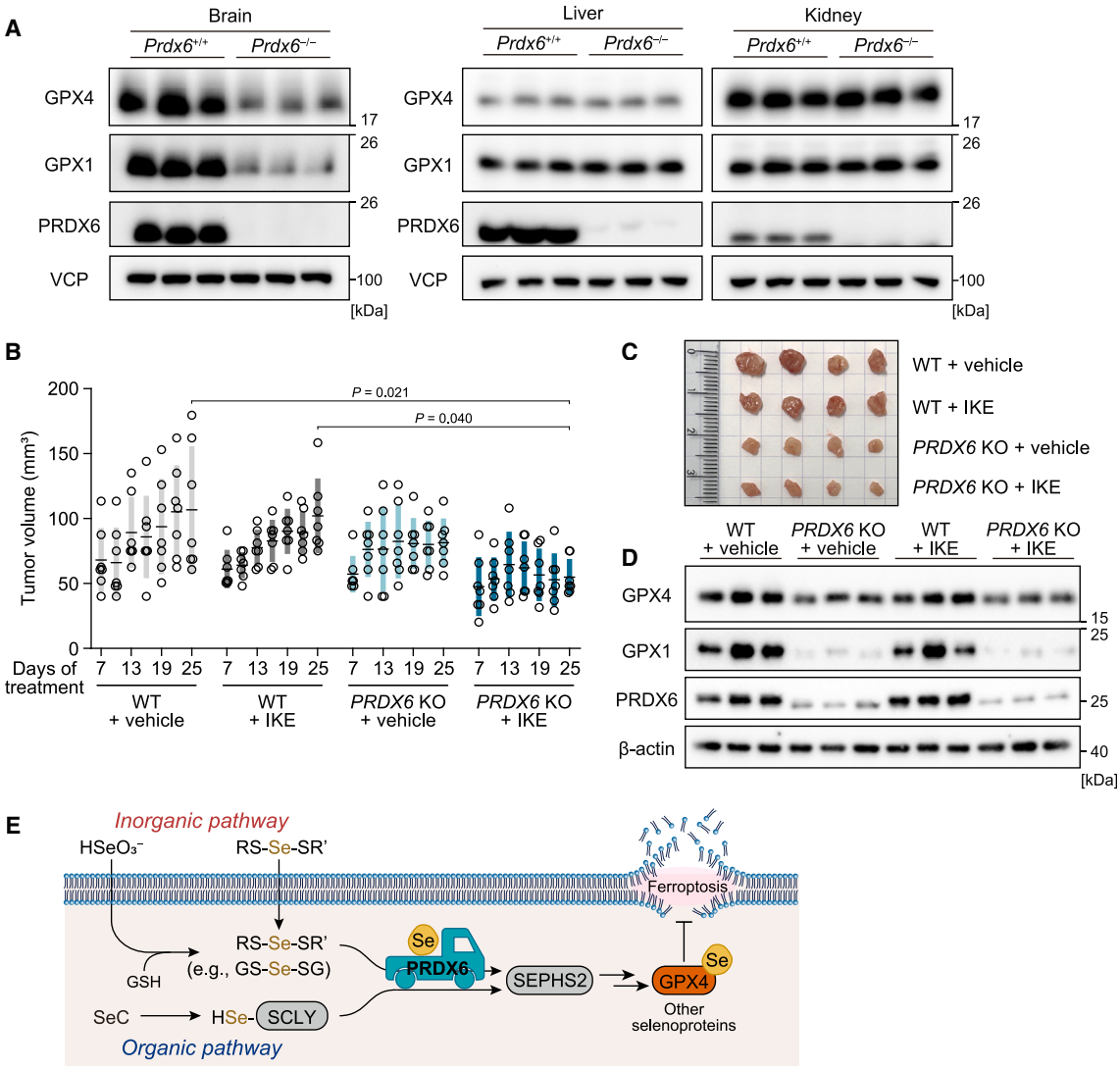

Figure 7. Physiological significance of PRDX6 as a crucial player in selenium utilization

(A) Immunoblot analysis of GPX4 and GPX1 in the whole brain, liver, and kidney collected from *Prdx6* knockout mice (*Prdx6*$^{-/-}$) and WT (*Prdx6*$^{+/+}$) mice.

(B) Growth curves of tumors derived from A549 cells in xenograft mouse models. WT or *PRDX6* KO A549 cells were subcutaneously implanted into BALB/c nude mice. A total of 4 days after implantation, mice were treated with vehicle or IKE (40 mg/kg/day daily i.p.) for 25 days. Mean ± SD of $n = 7$ (ANOVA, Tukey).

(C and D) Images (C) and immunoblot analysis (D) of the xenograft tumor derived from WT and *PRDX6* KO A549 cells (collected after 25 days of treatment with vehicle or IKE).

(E) Proposed model for the role of RPDX6 in intracellular selenium (Se) handling. Cellular selenium derived from the inorganic uptake pathway presumably forms RS-Se-SR' complex, such as GS-Se-SG, by reacting with GSH. PRDX6 reacts with GS-Se-SG, leading to the formation of PRDX6-Se adducts at the C47 residue, which act as a mobile selenium carrier. In the organic pathway, PRDX6 presumably bound to selenium derived from SCLY pathway. The PRDX6-bound selenium subsequently serves as the substrate for SEPHS2 and can be utilized as an efficient selenium source for the biosynthesis of selenoproteins, including GPX4, thereby suppressing ferroptosis.

of GPX4 in PRDX6-deficient xenograft tumors, even under normal diet feeding, could be due to proliferating tumors requiring higher selenium demands to maximize the expression of selenoproteins compared with normal tissue, or it is possible that the contribution of each selenium utilization pathway differs in cancer cells, resulting in a higher contribution of PRDX6 compared with normal tissues. Although *PRDX6* KO reduced GPX4 across a wide range of cultured cancer cells, the effect of *PRDX6* KO would likely vary depending on tumor type *in vivo*.

Loss of GPX4 and subsequent (phospho)lipid peroxidation are crucial triggers for ferroptosis induction. However, our results suggest that other proteins and/or molecules besides GPX4 and PRDX6 may also contribute to intracellular PCOOH reduction. Because glutathione S-transferase (GST), along with GSH, has been reported to be necessary for the efficient redox cycling of the peroxidase activity of PRDX6,[64] the present assay system, which lacks GST, may underestimate the PRDX6's PCOOH-reducing activity of PRDX6. Nonetheless,

our results suggest that, unexpectedly, GPX4 and PRDX6 do not contribute substantially to overall PCOOH reduction in cells. This raises the question of why GPX4 deletion alone triggers ferroptosis when enzymes other than GPX4 are also responsible for overall PCOOH reduction. Possible scenarios include the likelihood that other PLOOH species besides PCOOH are more critical for the execution of ferroptosis or that GPX4 plays a primary role in the reduction of PLOOH in certain organelles (e.g., at the plasma membrane) known to be critically involved in ferroptosis. Future research should therefore investigate the molecular identity responsible for cellular PLOOH reduction beyond GPX4 and PRDX6 and their role in ferroptosis regulation.

In summary, our study has identified the PRDX6-dependent selenium metabolism as a critical regulator for ferroptosis surveillance. Moreover, our findings that *PRDX6* deficiency sensitizes cancer cells to ferroptosis-inducing agents and that a *Prdx6*-deficient brain exhibits strongly reduced levels of GPX4 should spur future research in addressing this axis for potential applications in anti-cancer treatment and neurodegenerative disease.

Limitations of the study

Although our study proposes an important role for PRDX6 in ferroptosis regulation by impacting selenoprotein expression, several aspects still require further investigation. Mechanistically, although both PRDX6 C47 and C91 bind selenium in a GSH-dependent manner, the essential role of the C47 residue as a selenium-acceptor function is intriguing. This may be linked to how PRDX6 structurally interacts with SEPHS2, the immediate downstream recipient of selenium for selenophosphate synthesis. Unlike the LC-MS analysis, the ICP-MS measurements detected partial selenium binding to PRDX6 both in the absence of GSH and following NEM pretreatment (Figures 6D and S5D). This residual selenium binding is likely due to nonspecific interactions between selenium and the protein rather than covalent binding. Selenium attached through such nonspecific interactions could also have been recovered with the PRDX6 protein during the methanol-chloroform precipitation process. Another question is how PRDX6 utilizes supplemented selenium in GSH- and Cys-depleted conditions because GSH was required for PRDX6-selenium binding, at least in the cell-free reactions. The reasons for this are (1) the possibility that even minimal levels of GSH may be sufficient for PRDX6 to bind selenium even under decreased GSH conditions, (2) the possibility that complexes of selenium with other molecules may also serve as substrates besides GS-Se-SG, or (3) the possibility that PRDX6, in its oxidized form, which may occur under decreased reducing potential by depleting cellular GSH and Cys, might be able to directly bind selenium without GSH. Furthermore, it remains to be investigated whether GS-Se-SG is indeed present in cells and whether it is the predominant binding substrate for PRDX6 under cellular conditions, as well as observed under cell-free conditions. These questions highlight the need for additional research to further elucidate the role of PRDX6 in selenium metabolism and its implications for ferroptosis regulation.

RESOURCE AVAILABILITY

Lead contact

Further information and requests for resources and reagents should be directed to and will be fulfilled by the lead contact, Marcus Conrad (marcus.conrad@helmholtz-munich.de).

Materials availability

All reagents and materials are listed in the key resources table. Materials are available on reasonable request.

Data and code availability

- Original western blot images have been deposited at Mendeley Database and are publicly accessible via the DOI provided in the key resources table.
- This paper does not report the original code.
- Any further information needed to re-analyze the data reported in this paper is available from the lead contact upon request.

ACKNOWLEDGMENTS

We thank Dr. Christopher Horst Lillig (University Medicine Greifswald) for kindly providing antibodies against PRDX1 and PRDX2; Tomoki Kikkawa (Tohoku University) for supporting immunoblotting analysis of *Prdx6* KO mouse tissues; Dr. Ryuta Tobe (Tohoku University) and Dr. Sho Kobayashi (Yamagata University) for providing expert insight; and the Institute for Animal Experimentation, Tohoku University Graduate School of Medicine for the technical support in reproductive engineering techniques. This work was supported by the Deutsche Forschungsgemeinschaft (DFG) (CO 291/7-1, the Priority Program SPP 2306 [CO 291/9-1, #461385412; CO 291/10-1, #461507177], and the CRC TRR 353 [CO 291/11-1; #471011418]); the German Federal Ministry of Education and Research (BMBF) FERROPATH (01EJ2205B); the European Research Council (ERC) under the European Union's Horizon 2020 research and innovation programme (grant agreement no. GA 884754) to M.C.; research grant of Sapporo Bioscience Foundation and Food Science Institute Foundation (Ryoshoku Kenkyuukai) to E.M.; and JSPS KAKENHI (20KK0363 and 18K08198 to E.M., 22KK0253 to J.I., and 22H02278 to J.I. and K.N.). Figures 1A and 5A were created with BioRender.com.

AUTHOR CONTRIBUTIONS

Conceptualization, J.I., T.N., E.M., and M.C.; investigation, T.N., T.T., D.C., C.B., G.P., A.S.D.M., M.S., W.Z., J.Z., N.Y., K.O., and Y.O.; resources, M.Y., Y.K., and M.A.; data curation, T.D.; supervision, S.D., B.P., H.S., Y.S., and K.N.; writing—original draft, review, and editing, J.I., T.N., E.M., A.W., and M.C; funding acquisition, J.I., E.M., K.N., and M.C.

DECLARATION OF INTERESTS

M.C. is a co-founder and shareholder of ROSCUE Therapeutics GmbH. M.C., B.P., and T.N. hold patents for some of the compounds described herein. M.C. is a member of the journal advisory board.

STAR★METHODS

Detailed methods are provided in the online version of this paper and include the following:

- KEY RESOURCES TABLE
- EXPERIMENTAL MODEL AND STUDY PARTICIPANT DETAILS
  - Cells
  - Animals
- METHOD DETAILS
  - Chemicals
  - Lentiviral production and transduction

SUPPLEMENTAL INFORMATION

Supplemental information can be found online at https://doi.org/10.1016/j.molcel.2024.10.028.

Received: April 10, 2024
Revised: July 29, 2024
Accepted: October 23, 2024
Published: November 14, 2024

REFERENCES

1. Dixon, S.J., Lemberg, K.M., Lamprecht, M.R., Skouta, R., Zaitsev, E.M., Gleason, C.E., Patel, D.N., Bauer, A.J., Cantley, A.M., Yang, W.S., et al. (2012). Ferroptosis: an iron-dependent form of nonapoptotic cell death. Cell *149*, 1060–1072. https://doi.org/10.1016/j.cell.2012.03.042.
2. Dixon, S.J., and Olzmann, J.A. (2024). The cell biology of ferroptosis. Nat. Rev. Mol. Cell Biol. *25*, 424–442. https://doi.org/10.1038/s41580-024-00703-5.
3. Mishima, E., and Conrad, M. (2022). Nutritional and metabolic control of ferroptosis. Annu. Rev. Nutr. *42*, 275–309. https://doi.org/10.1146/annurev-nutr-062320-114541.
4. Berndt, C., Alborzinia, H., Amen, V.S., Ayton, S., Barayeu, U., Bartelt, A., Bayir, H., Bebber, C.M., Birsoy, K., Böttcher, J.P., et al. (2024). Ferroptosis in health and disease. Redox Biol. *75*, 103211. https://doi.org/10.1016/j.redox.2024.103211.
5. Viswanathan, V.S., Ryan, M.J., Dhruv, H.D., Gill, S., Eichhoff, O.M., Seashore-Ludlow, B., Kaffenberger, S.D., Eaton, J.K., Shimada, K., Aguirre, A.J., et al. (2017). Dependency of a therapy-resistant state of cancer cells on a lipid peroxidase pathway. Nature *547*, 453–457. https://doi.org/10.1038/nature23007.
6. Wang, W., Green, M., Choi, J.E., Gijón, M., Kennedy, P.D., Johnson, J.K., Liao, P., Lang, X., Kryczek, I., Sell, A., et al. (2019). CD8+ T cells regulate tumour ferroptosis during cancer immunotherapy. Nature *569*, 270–274. https://doi.org/10.1038/s41586-019-1170-y.
7. Rodriguez, R., Schreiber, S.L., and Conrad, M. (2022). Persister cancer cells: Iron addiction and vulnerability to ferroptosis. Mol. Cell *82*, 728–740. https://doi.org/10.1016/j.molcel.2021.12.001.
8. Nakamura, T., and Conrad, M. (2024). Exploiting ferroptosis vulnerabilities in cancer. Nat. Cell Biol. *26*, 1407–1419. https://doi.org/10.1038/s41556-024-01425-8.
9. Hirata, Y., and Mishima, E. (2024). Membrane dynamics and cation handling in ferroptosis. Physiology *39*, 73–87. https://doi.org/10.1152/physiol.00029.2023.
10. Li, Z., Lange, M., Dixon, S.J., and Olzmann, J.A. (2024). Lipid quality control and ferroptosis: From concept to mechanism. Annu. Rev. Biochem. *93*, 499–528. https://doi.org/10.1146/annurev-biochem-052521-033527.
11. Friedmann Angeli, J.P., Schneider, M., Proneth, B., Tyurina, Y.Y., Tyurin, V.A., Hammond, V.J., Herbach, N., Aichler, M., Walch, A., Eggenhofer, E., et al. (2014). Inactivation of the ferroptosis regulator Gpx4 triggers acute renal failure in mice. Nat. Cell Biol. *16*, 1180–1191. https://doi.org/10.1038/ncb3064.
12. Yang, W.S., SriRamaratnam, R., Welsch, M.E., Shimada, K., Skouta, R., Viswanathan, V.S., Cheah, J.H., Clemons, P.A., Shamji, A.F., Clish, C.B., et al. (2014). Regulation of ferroptotic cancer cell death by GPX4. Cell *156*, 317–331. https://doi.org/10.1016/j.cell.2013.12.010.
13. Ingold, I., Berndt, C., Schmitt, S., Doll, S., Poschmann, G., Buday, K., Roveri, A., Peng, X., Porto Freitas, F., Seibt, T., et al. (2018). Selenium utilization by GPX4 is required to prevent hydroperoxide-induced ferroptosis. Cell *172*, 409–422.e21. https://doi.org/10.1016/j.cell.2017.11.048.
14. Mishima, E., Ito, J., Wu, Z., Nakamura, T., Wahida, A., Doll, S., Tonnus, W., Nepachalovich, P., Eggenhofer, E., Aldrovandi, M., et al. (2022). A non-canonical vitamin K cycle is a potent ferroptosis suppressor. Nature *608*, 778–783. https://doi.org/10.1038/s41586-022-05022-3.
15. Doll, S., Freitas, F.P., Shah, R., Aldrovandi, M., da Silva, M.C., Ingold, I., Goya Grocin, A., Xavier da Silva, T.N., Panzilius, E., Scheel, C.H., et al. (2019). FSP1 is a glutathione-independent ferroptosis suppressor. Nature *575*, 693–698. https://doi.org/10.1038/s41586-019-1707-0.
16. Bersuker, K., Hendricks, J.M., Li, Z., Magtanong, L., Ford, B., Tang, P.H., Roberts, M.A., Tong, B., Maimone, T.J., Zoncu, R., et al. (2019). The CoQ oxidoreductase FSP1 acts parallel to GPX4 to inhibit ferroptosis. Nature *575*, 688–692. https://doi.org/10.1038/s41586-019-1705-2.
17. Kraft, V.A.N., Bezjian, C.T., Pfeiffer, S., Ringelstetter, L., Müller, C., Zandkarimi, F., Merl-Pham, J., Bao, X., Anastasov, N., Kössl, J., et al. (2020). GTP cyclohydrolase 1/tetrahydrobiopterin counteract ferroptosis through lipid remodeling. ACS Cent. Sci. *6*, 41–53. https://doi.org/10.1021/acscentsci.9b01063.
18. Soula, M., Weber, R.A., Zilka, O., Alwaseem, H., La, K., Yen, F., Molina, H., Garcia-Bermudez, J., Pratt, D.A., and Birsoy, K. (2020). Metabolic determinants of cancer cell sensitivity to canonical ferroptosis inducers. Nat. Chem. Biol. *16*, 1351–1360. https://doi.org/10.1038/s41589-020-0613-y.
19. Yamada, N., Karasawa, T., Ito, J., Yamamuro, D., Morimoto, K., Nakamura, T., Komada, T., Baatarjav, C., Saimoto, Y., Jinnouchi, Y., et al. (2024). Inhibition of 7-dehydrocholesterol reductase prevents hepatic ferroptosis under an active state of sterol synthesis. Nat. Commun. *15*, 2195. https://doi.org/10.1038/s41467-024-46386-6.
20. Li, Y., Ran, Q., Duan, Q., Jin, J., Wang, Y., Yu, L., Wang, C., Zhu, Z., Chen, X., Weng, L., et al. (2024). 7-Dehydrocholesterol dictates ferroptosis sensitivity. Nature *626*, 411–418. https://doi.org/10.1038/s41586-023-06983-9.
21. Freitas, F.P., Alborzinia, H., dos Santos, A.F., Nepachalovich, P., Pedrera, L., Zilka, O., Inague, A., Klein, C., Aroua, N., Kaushal, K., et al. (2024). 7-Dehydrocholesterol is an endogenous suppressor of ferroptosis. Nature *626*, 401–410. https://doi.org/10.1038/s41586-023-06878-9.
22. Fisher, A.B., Dodia, C., Manevich, Y., Chen, J.W., and Feinstein, S.I. (1999). Phospholipid hydroperoxides are substrates for non-selenium glutathione peroxidase. J. Biol. Chem. *274*, 21326–21334. https://doi.org/10.1074/jbc.274.30.21326.
23. Manevich, Y., Sweitzer, T., Pak, J.H., Feinstein, S.I., Muzykantov, V., and Fisher, A.B. (2002). 1-Cys peroxiredoxin overexpression protects cells against phospholipid peroxidation-mediated membrane damage. Proc.

Natl. Acad. Sci. USA *99*, 11599–11604. https://doi.org/10.1073/pnas.182384499.

24. Chen, J.W., Dodia, C., Feinstein, S.I., Jain, M.K., and Fisher, A.B. (2000). 1-Cys peroxiredoxin, a bifunctional enzyme with glutathione peroxidase and phospholipase A2 activities. J. Biol. Chem. *275*, 28421–28427. https://doi.org/10.1074/jbc.M005073200.
25. Manevich, Y., Reddy, K.S., Shuvaeva, T., Feinstein, S.I., and Fisher, A.B. (2007). Structure and phospholipase function of peroxiredoxin 6: identification of the catalytic triad and its role in phospholipid substrate binding1. J. Lipid Res. *48*, 2306–2318. https://doi.org/10.1194/jlr.M700299-JLR200.
26. Lu, B., Chen, X.-B., Hong, Y.-C., Zhu, H., He, Q.-J., Yang, B., Ying, M.-D., and Cao, J. (2019). Identification of PRDX6 as a regulator of ferroptosis. Acta Pharmacol. Sinica *40*, 1334–1342. https://doi.org/10.1038/s41401-019-0233-9.
27. Liu, J., Sun, L., Chen, D., Huo, X., Tian, X., Li, J., Liu, M., Yu, Z., Zhang, B., Yang, Y., et al. (2022). Prdx6-induced inhibition of ferroptosis in epithelial cells contributes to liquiritin-exerted alleviation of colitis. Food Funct. *13*, 9470–9480. https://doi.org/10.1039/D2FO00945E.
28. Torres-Velarde, J.M., Allen, K.N., Salvador-Pascual, A., Leija, R.G., Luong, D., Moreno-Santillán, D.D., Ensminger, D.C., and Vázquez-Medina, J.P. (2024). Peroxiredoxin 6 suppresses ferroptosis in lung endothelial cells. Free Radic. Biol. Med. *218*, 82–93. https://doi.org/10.1016/j.freeradbiomed.2024.04.208.
29. Li, Z., Ferguson, L., Deol, K.K., Roberts, M.A., Magtanong, L., Hendricks, J.M., Mousa, G.A., Kilinc, S., Schaefer, K., Wells, J.A., et al. (2022). Ribosome stalling during selenoprotein translation exposes a ferroptosis vulnerability. Nat. Chem. Biol. *18*, 751–761. https://doi.org/10.1038/s41589-022-01033-3.
30. Nakamura, T., Ito, J., Mourão, A.S.D., Wahida, A., Nakagawa, K., Mishima, E., and Conrad, M. (2024). A tangible method to assess native ferroptosis suppressor activity. Cell Rep. Methods *4*, 100710. https://doi.org/10.1016/j.crmeth.2024.100710.
31. Seiler, A., Schneider, M., Förster, H., Roth, S., Wirth, E.K., Culmsee, C., Plesnila, N., Kremmer, E., Rådmark, O., Wurst, W., et al. (2008). Glutathione peroxidase 4 senses and translates oxidative stress into 12/15-lipoxygenase dependent- and AIF-mediated cell death. Cell Metab. *8*, 237–248. https://doi.org/10.1016/j.cmet.2008.07.005.
32. Wood, Z.A., Schröder, E., Robin Harris, J., and Poole, L.B. (2003). Structure, mechanism and regulation of peroxiredoxins. Trends Biochem. Sci. *28*, 32–40. https://doi.org/10.1016/S0968-0004(02)00003-8.
33. Liang, C., Zhang, X., Yang, M., and Dong, X. (2019). Recent progress in ferroptosis inducers for cancer therapy. Adv. Mater. *31*, e1904197. https://doi.org/10.1002/adma.201904197.
34. Nakamura, T., Mishima, E., Yamada, N., Mourão, A.S.D., Trümbach, D., Doll, S., Wanninger, J., Lytton, E., Sennhenn, P., Nishida Xavier da Silva, T., et al. (2023). Integrated chemical and genetic screens unveil FSP1 mechanisms of ferroptosis regulation. Nat. Struct. Mol. Biol. *30*, 1806–1815. https://doi.org/10.1038/s41594-023-01136-y.
35. Nakamura, T., Hipp, C., Santos Dias Mourão, A., Borggräfe, J., Aldrovandi, M., Henkelmann, B., Wanninger, J., Mishima, E., Lytton, E., Emler, D., et al. (2023). Phase separation of FSP1 promotes ferroptosis. Nature *619*, 371–377. https://doi.org/10.1038/s41586-023-06255-6.
36. Tsherniak, A., Vazquez, F., Montgomery, P.G., Weir, B.A., Kryukov, G., Cowley, G.S., Gill, S., Harrington, W.F., Pantel, S., Krill-Burger, J.M., et al. (2017). Defining a Cancer Dependency Map. Cell *170*, 564–576.e16. https://doi.org/10.1016/j.cell.2017.06.010.
37. Amici, D.R., Jackson, J.M., Truica, M.I., Smith, R.S., Abdulkadir, S.A., and Mendillo, M.L. (2021). FIREWORKS: a bottom-up approach to integrative coessentiality network analysis. Life Sci. Alliance *4*, e202000882. https://doi.org/10.26508/lsa.202000882.
38. Conrad, M., and Proneth, B. (2020). Selenium: Tracing Another Essential Element of Ferroptotic Cell Death. Cell Chem. Biol. *27*, 409–419. https://doi.org/10.1016/j.chembiol.2020.03.012.
39. Brigelius-Flohé, R., and Maiorino, M. (2013). Glutathione peroxidases. Biochim. Biophys. Acta *1830*, 3289–3303. https://doi.org/10.1016/j.bbagen.2012.11.020.
40. Xu, X.M., Turanov, A.A., Carlson, B.A., Yoo, M.H., Everley, R.A., Nandakumar, R., Sorokina, I., Gygi, S.P., Gladyshev, V.N., and Hatfield, D.L. (2010). Targeted insertion of cysteine by decoding UGA codons with mammalian selenocysteine machinery. Proc. Natl. Acad. Sci. USA *107*, 21430–21434. https://doi.org/10.1073/pnas.1009947107.
41. Chatterjee, S., Feinstein, S.I., Dodia, C., Sorokina, E., Lien, Y.-C., Nguyen, S., Debolt, K., Speicher, D., and Fisher, A.B. (2011). Peroxiredoxin 6 phosphorylation and subsequent phospholipase A_2 activity are required for agonist-mediated activation of NADPH oxidase in mouse pulmonary microvascular endothelium and alveolar macrophages. J. Biol. Chem. *286*, 11696–11706. https://doi.org/10.1074/jbc.M110.206623.
42. dos Santos, A.F., Fazeli, G., Xavier da Silva, T.N., and Friedmann Angeli, J.P. (2023). Ferroptosis: mechanisms and implications for cancer development and therapy response. Trends Cell Biol. *33*, 1062–1076. https://doi.org/10.1016/j.tcb.2023.04.005.
43. Alborzinia, H., Chen, Z., Yildiz, U., Freitas, F.P., Vogel, F.C.E., Varga, J.P., Batani, J., Bartenhagen, C., Schmitz, W., Büchel, G., et al. (2023). LRP8-mediated selenocysteine uptake is a targetable vulnerability in MYCN-amplified neuroblastoma. EMBO Mol. Med. *15*, e18014. https://doi.org/10.15252/emmm.202318014.
44. Shimomura, T., Hirakawa, N., Ohuchi, Y., Ishiyama, M., Shiga, M., and Ueno, Y. (2021). Simple fluorescence assay for cystine uptake via the xCT in cells using selenocystine and a fluorescent probe. ACS Sens. *6*, 2125–2128. https://doi.org/10.1021/acssensors.1c00496.
45. Tobe, R., and Mihara, H. (2018). Delivery of selenium to selenophosphate synthetase for selenoprotein biosynthesis. Biochim. Biophys. Acta Gen. Subj. *1862*, 2433–2440. https://doi.org/10.1016/j.bbagen.2018.05.023.
46. Mizuno, A., Toyama, T., Ichikawa, A., Sakai, N., Yoshioka, Y., Nishito, Y., Toga, R., Amesaka, H., Kaneko, T., Arisawa, K., et al. (2023). An efficient selenium transport pathway of selenoprotein P utilizing a high-affinity $ApoER_2$ receptor variant and being independent of selenocysteine lyase. J. Biol. Chem. *299*, 105009. https://doi.org/10.1016/j.jbc.2023.105009.
47. Olm, E., Fernandes, A.P., Hebert, C., Rundlöf, A.-K., Larsen, E.H., Danielsson, O., and Björnstedt, M. (2009). Extracellular thiol-assisted selenium uptake dependent on the x_c^- cystine transporter explains the cancer-specific cytotoxicity of selenite. Proc. Natl. Acad. Sci. USA *106*, 11400–11405. https://doi.org/10.1073/pnas.0902204106.
48. Lee, N., Park, S.J., Lange, M., Tseyang, T., Doshi, M.B., Kim, T.Y., Song, Y., Kim, D.I., Greer, P.L., Olzmann, J.A., et al. (2024). Selenium reduction of ubiquinone via SQOR suppresses ferroptosis. Nat. Metab. *6*, 343–358. https://doi.org/10.1038/s42255-024-00974-4.
49. Banjac, A., Perisic, T., Sato, H., Seiler, A., Bannai, S., Weiss, N., Kölle, P., Tschoep, K., Issels, R.D., Daniel, P.T., et al. (2008). The cystine/cysteine cycle: a redox cycle regulating susceptibility versus resistance to cell death. Oncogene *27*, 1618–1628. https://doi.org/10.1038/sj.onc.1210796.
50. Mandal, P.K., Seiler, A., Perisic, T., Kölle, P., Banjac Canak, A., Förster, H., Weiss, N., Kremmer, E., Lieberman, M.W., Bannai, S., et al. (2010). System x_c^- and thioredoxin reductase 1 cooperatively rescue glutathione deficiency. J. Biol. Chem. *285*, 22244–22253. https://doi.org/10.1074/jbc.M110.121327.
51. Conrad, M., and Sato, H. (2012). The oxidative stress-inducible cystine/glutamate antiporter, system x c -: Cystine supplier and beyond. Amino Acids *42*, 231–246.
52. Kobayashi, S., Ikeda, Y., Shigeno, Y., Konno, H., and Fujii, J. (2020). γ-Glutamylcysteine synthetase and γ-glutamyl transferase as differential enzymatic sources of γ-glutamylpeptides in mice. Amino Acids *52*, 555–566. https://doi.org/10.1007/s00726-020-02835-2.
53. Homma, T., Kobayashi, S., Sato, H., and Fujii, J. (2019). Edaravone, a free radical scavenger, protects against ferroptotic cell death in vitro. Exp. Cell Res. *384*, 111592. https://doi.org/10.1016/j.yexcr.2019.111592.

54. Ganther, H.E. (1971). Reduction of the selenotrisulfide derivative of glutathione to a persulfide analog by glutathione reductase. Biochemistry *10*, 4089–4098. https://doi.org/10.1021/bi00798a013.

55. Mo, Y., Feinstein, S.I., Manevich, Y., Zhang, Q., Lu, L., Ho, Y.S., and Fisher, A.B. (2003). 1-Cys peroxiredoxin knock-out mice express mRNA but not protein for a highly related intronless gene. FEBS Lett. *555*, 192–198. https://doi.org/10.1016/s0014-5793(03)01199-2.

56. Zhang, Y., Tan, H., Daniels, J.D., Zandkarimi, F., Liu, H., Brown, L.M., Uchida, K., O'Connor, O.A., and Stockwell, B.R. (2019). Imidazole ketone erastin induces ferroptosis and slows tumor growth in a mouse lymphoma model. Cell Chem. Biol. *26*, 623–633.e9. https://doi.org/10.1016/j.chembiol.2019.01.008.

57. Falnoga, I., and Tušek-Žnidarič, M. (2007). Selenium–mercury interactions in man and animals. Biol. Trace Elem. Res. *119*, 212–220. https://doi.org/10.1007/s12011-007-8009-3.

58. Fujita, H., Tanaka, Y.-K., Ogata, S., Suzuki, N., Kuno, S., Barayeu, U., Akaike, T., Ogra, Y., and Iwai, K. (2024). PRDX6 augments selenium utilization to limit iron toxicity and ferroptosis. Nat. Struct. Mol. Biol. *31*, 1277–1285. https://doi.org/10.1038/s41594-024-01329-z.

59. Chen, Z., Inague, A., Kaushal, K., Fazeli, G., Xavier da Silva, T.N., Ferreira Dos Santos, A., Cheytan, T., Freitas, F.P., Yildiz, U., Viviani, L.G., et al. (2024). PRDX6 contributes to selenocysteine metabolism and ferroptosis resistance. Mol. Cell *84*, this.issue. https://doi.org/10.1016/j.molcel.2024.10.028.

60. Sunde, R.A., Li, J.-L., and Taylor, R.M. (2016). Insights for setting of nutrient requirements, Gleaned by comparison of selenium status biomarkers in turkeys and chickens versus rats, mice, and lambs. Adv. Nutr. *7*, 1129–1138. https://doi.org/10.3945/an.116.012872.

61. Li, J.-L., and Sunde, R.A. (2016). Selenoprotein transcript level and enzyme activity as biomarkers for selenium status and selenium requirements of chickens (Gallus gallus). PLoS one *11*, e0152392. https://doi.org/10.1371/journal.pone.0152392.

62. Hill, K.E., Zhou, J., McMahan, W.J., Motley, A.K., and Burk, R.F. (2004). Neurological dysfunction occurs in mice with targeted deletion of the selenoprotein P gene. J. Nutr. *134*, 157–161. https://doi.org/10.1093/jn/134.1.157.

63. Hill, K.E., Zhou, J., McMahan, W.J., Motley, A.K., Atkins, J.F., Gesteland, R.F., and Burk, R.F. (2003). Deletion of selenoprotein P alters distribution of selenium in the mouse. J. Biol. Chem. *278*, 13640–13646. https://doi.org/10.1074/jbc.M300755200.

64. Ralat, L.A., Manevich, Y., Fisher, A.B., and Colman, R.F. (2006). Direct evidence for the formation of a complex between 1-cysteine peroxiredoxin and glutathione S-transferase pi with activity changes in both enzymes. Biochemistry *45*, 360–372. https://doi.org/10.1021/bi0520737.

65. Godoy, J.R., Funke, M., Ackermann, W., Haunhorst, P., Oesteritz, S., Capani, F., Elsässer, H.-P., and Lillig, C.H. (2011). Redox atlas of the mouse: Immunohistochemical detection of glutaredoxin-, peroxiredoxin-, and thioredoxin-family proteins in various tissues of the laboratory mouse. Biochim. Biophys. Acta *1810*, 2–92. https://doi.org/10.1016/j.bbagen.2010.05.006.

66. Gascón, S., Murenu, E., Masserdotti, G., Ortega, F., Russo, G.L., Petrik, D., Deshpande, A., Heinrich, C., Karow, M., Robertson, S.P., et al. (2016). Identification and successful negotiation of a metabolic checkpoint in direct neuronal reprogramming. Cell Stem Cell *18*, 396–409. https://doi.org/10.1016/j.stem.2015.12.003.

67. Mishima, E., Nakamura, T., Zheng, J., Zhang, W., Mourão, A.S.D., Sennhenn, P., and Conrad, M. (2023). DHODH inhibitors sensitize to ferroptosis by FSP1 inhibition. Nature *619*, E9–E18. https://doi.org/10.1038/s41586-023-06269-0.

68. Ito, J., Mizuochi, S., Nakagawa, K., Kato, S., and Miyazawa, T. (2015). Tandem mass spectrometry analysis of linoleic and arachidonic acid hydroperoxides via promotion of alkali metal adduct formation. Anal. Chem. *87*, 4980–4987. https://doi.org/10.1021/acs.analchem.5b00851.

69. Ito, J., Komuro, M., Parida, I.S., Shimizu, N., Kato, S., Meguro, Y., Ogura, Y., Kuwahara, S., Miyazawa, T., and Nakagawa, K. (2019). Evaluation of lipid oxidation mechanisms in beverages and cosmetics via analysis of lipid hydroperoxide isomers. Sci. Rep. *9*, 7387. https://doi.org/10.1038/s41598-019-43645-1.

70. Folch, J., Lees, M., and Sloane Stanley, G.H. (1957). A simple method for the isolation and purification of total lipides from animal tissues. J. Biol. Chem. *226*, 497–509.

71. Ito, J., Nakagawa, K., Kato, S., Miyazawa, T., Kimura, F., and Miyazawa, T. (2016). The combination of maternal and offspring high-fat diets causes marked oxidative stress and development of metabolic syndrome in mouse offspring. Life Sci. *151*, 70–75. https://doi.org/10.1016/j.lfs.2016.02.089.

72. Kobayashi, E., Ito, J., Shimizu, N., Kokumai, T., Kato, S., Sawada, K., Hashimoto, H., Eitsuka, T., Miyazawa, T., and Nakagawa, K. (2019). Evaluation of γ-oryzanol accumulation and lipid metabolism in the body of mice following long-term administration of γ-oryzanol. Nutrients *11*, 104.

73. Ito, J., Nakagawa, K., Kato, S., Hirokawa, T., Kuwahara, S., Nagai, T., and Miyazawa, T. (2015). Direct separation of the diastereomers of phosphatidylcholine hydroperoxide bearing 13-hydroperoxy-9Z,11E-octadecadienoic acid using chiral stationary phase high-performance liquid chromatography. J. Chromatogr. A *1386*, 53–61. https://doi.org/10.1016/j.chroma.2015.01.080.

74. Kato, S., Nakagawa, K., Suzuki, Y., Asai, A., Nagao, M., Nagashima, K., Oikawa, S., and Miyazawa, T. (2015). Liquid chromatography-tandem mass spectrometry determination of human plasma 1-palmitoyl-2-hydroperoxyoctadecadienoyl-phosphatidylcholine isomers via promotion of sodium adduct formation. Anal. Biochem. *471*, 51–60. https://doi.org/10.1016/j.ab.2014.10.017.

75. Yamada, N., Karasawa, T., Kimura, H., Watanabe, S., Komada, T., Kamata, R., Sampilvanjil, A., Ito, J., Nakagawa, K., Kuwata, H., et al. (2020). Ferroptosis driven by radical oxidation of n-6 polyunsaturated fatty acids mediates acetaminophen-induced acute liver failure. Cell Death Dis. *11*, 144. https://doi.org/10.1038/s41419-020-2334-2.

76. Saito, Y., Yoshida, Y., Akazawa, T., Takahashi, K., and Niki, E. (2003). Cell death caused by selenium deficiency and protective effect of antioxidants. J. Biol. Chem. *278*, 39428–39434. https://doi.org/10.1074/jbc.M305542200.

77. Kim, K.H., Lee, W., and Kim, E.E. (2016). Crystal structures of human peroxiredoxin 6 in different oxidation states. Biochem. Biophys. Res. Commun. *477*, 717–722. https://doi.org/10.1016/j.bbrc.2016.06.125.

78. Prescher, N., Hänsch, S., Knobbe-Thomsen, C.B., Stühler, K., and Poschmann, G. (2021). The migration behavior of human glioblastoma cells is influenced by the redox-sensitive human macrophage capping protein CAPG. Free Radic. Biol. Med. *167*, 81–93. https://doi.org/10.1016/j.freeradbiomed.2021.02.038.

79. Fleischer, H., Glang, S., Schollmeyer, D., Mitzel, N.W., and Bühl, M. (2004). Experimental investigations and ab initio studies of selenium(ii) dialkanethiolates, Se(SR)2. Dalton Trans. *21*, 3765–3771. https://doi.org/10.1039/B409726B.

80. Takayama, N., Iwamoto, N., Sumi, D., Shinkai, Y., Tanaka-Kagawa, T., Jinno, H., and Kumagai, Y. (2011). Peroxiredoxin 6 is a molecular target for 1,2-naphthoquinone, an atmospheric electrophile, in human pulmonary epithelial A549 cells. J. Toxicol. Sci. *36*, 817–821. https://doi.org/10.2131/jts.36.817.

Please cite this article in press as: Ito et al., PRDX6 dictates ferroptosis sensitivity by directing cellular selenium utilization, Molecular Cell (2024), https://doi.org/10.1016/j.molcel.2024.10.028

STAR★METHODS

KEY RESOURCES TABLE

REAGENT or RESOURCE	SOURCE	IDENTIFIER
Antibodies		
Rabbit monoclonal anti-GPX4 (1:1000)	Abcam	Cat# ab125066; RRID: AB_10973901
Mouse monoclonal anti-FSP1 (1:1000)	Santa Cruz	Cat# sc-377120; RRID: AB_2893240
Rabbit polyclonal anti-GPX1 (1:1000)	Abcam	Cat# ab22604; RRID: AB_2112120
Rabbit anti-PRDX1 (1:1000)	Godoy et al.[65]	N/A
Rabbit anti-PRDX2 (1:1000)	Gascón et al.[66]	N/A
Rabbit monoclonal anti-PRDX3 (1:1000)	Abcam	Cat# ab129206 RRID: AB_11150432
Rabbit monoclonal anti-PRDX4 (1:1000)	Abcam	Cat# ab184167
Rabbit monoclonal anti-PRDX5 (1:1000)	Abcam	Cat# ab180587 RRID: AB_2904214
Rabbit anti-PRDX6 (1:1000)	Cell Signaling Technology	Cat# 95336 RRID: AB_2800244
Rabbit polyclonal anti-SELENOT (1:500)	Sigma Aldrich	Cat# HPA039780 RRID: AB_10805594
Rabbit polyclonal anti-SELENOS (1:500)	Sigma Aldrich	Cat# HPA010025 RRID: AB_1079900
Rabbit polyclonal anti-SEPHS2 (1:500)	Proteintech	Cat# 14109-1-AP RRID: AB_2878014
Rabbit monoclonal anti-TXNRD1 (1:1000)	Abcam	Cat# ab124954 RRID: AB_10975643
Rabbit monoclonal anti-TXNRD2 (1:1000)	Abcam	Cat# ab180493 RRID: AB_2732914
Mouse monoclonal anti-β-actin-HRP (1:5000)	Sigma Aldrich	Cat# A3854 RRID: AB_262011
Rabbit monoclonal anti-VCP (1:10000)	Abcam	Cat# ab11433 RRID: AB_298039
Rat IgG1 anti-HA (1:1000)	In house	Clone 3F10
Goat anti-rabbit-IgG-HRP (1:3000)	Cell Signaling	Cat# 7074S RRID: AB_2099233
Horse anti-mouse-IgG-HRP (1:3000)	Cell Signaling	Cat# 7076S RRID: AB_330924
Biological samples		
Liver tissue samples of Alb-CreERT2;*Gpx4*$^{fl/fl}$ (hepatocyte-specific *Gpx4* KO) mice	Mishima et al.[14]	N/A
Liver tissue samples of Cre(-);*Gpx4*$^{fl/fl}$ mice	Mishima et al.[14]	N/A
Chemicals, peptides, and recombinant proteins		
(*1S,3R*)-RSL3 (RSL3)	Cayman	Cat# Cay19288
Erastin	Merck	Cat# 329600
L-Buthionine sulfoximine (BSO)	Sigma Aldrich	Cat# B2515
4-Hydroxytamoxifen (4-OH TAM)	Sigma Aldrich	Cat# H7904
ML210	Cayman	Cat# 23282
FIN56	Cayman	Cat# 25180
FINO2	Cayman	Cat# 25096
Auranofin	Sigma Aldrich	Cat# A6733
Sulfasalazine	Sigma Aldrich	Cat# S0883
iFSP1	Cayman	Cat# 29483

(*Continued on next page*)

Please cite this article in press as: Ito et al., PRDX6 dictates ferroptosis sensitivity by directing cellular selenium utilization, Molecular Cell (2024), https://doi.org/10.1016/j.molcel.2024.10.028

Continued

REAGENT or RESOURCE	SOURCE	IDENTIFIER
viFSP1	Vistas-lab	Cat# STK626779
icFSP1	Intonation Research Laboratories	N/A
Imidazole ketone erastin (IKE)	Selleckchem	Cat# S8877
Liproxstatin-1 (Lip-1)	Selleckchem	Cat# S7699
L-Glutathione (GSH)	Sigma Aldrich	Cat# G4251
L-Glutathione oxidized (GSSG)	WAKO	Cat# 79-03333
Seleno-diglutathione (GS-Se-SG)	This study	N/A
N-ethylmaleimide (NEM)	Nacalai Tesque	Cat# 15512-11
Resazurin sodium salt	Sigma Aldrich	Cat# R7017
Sodium selenite (Na_2SeO_3)	Sigma Aldrich	Cat# S5261
L-Selenocystine (Sec2)	Sigma Aldrich	Cat# 545996
L-Selenomethionine (SeM)	Sigma Aldrich	Cat# S3132
MJ33	Cayman	Cat# 90001844
Rose bengal	Wako	Cat# 184-00272
PEI MAX	Polysciences	Cat# 24765
1-stearoyl-2-linoleoyl-sn-glycero-3-phosphoethanolamine (16:0/18:2 PE)	Avanti	Cat# 850802C
Iodomethane-d_3	Isotec	Cat# 176036
Deuterium-labelled phosphatidylcholine hydroperoxide (PCOOH-d_9)	This study	N/A
Insulin	Gibco	Cat# 12585014
Transferrin	Sigma Aldrich	Cat# T3309
Recombinant human PRDX6	This study	N/A
Recombinant human PRDX6 C47S	This study	N/A
Critical commercial assays		
Cytotoxicity Detection kit (LDH assay kit)	Roche	Cat# 11644793001
KOD -plus- Mutagenesis Kit	TOYOBO	Cat# SMK-101
Deposited data		
Western blots and microscopy images	This study	Mendeley Data: https://doi.org/10.17632/d2wzfr4twp.3
Experimental models: Cell lines		
Human: HEK293T	ATCC	CRL-1619
Human: HT-1080	ATCC	CCL-121
Human: 786-O	ATCC	CRL-1932
Human: A375	ATCC	CRL-1619
Human: A549	ATCC	CCL-185
Human: NCI-H460	ATCC	HTB-177
Human: LOX-IMVI	NCI/NIH	CVCL_1381
Human: HEC151	JCRB	JCRB1122-A
Human: HT-1080 *GPX4* KO	Mishima et al.[14]	N/A
Human: HT-1080 *GPX4* KO + hGPX4 short form OE	Mishima et al.[67]	N/A
Human: HT-1080 *PRDX6* KO	This paper	N/A
Human: HT-1080 *PRDX1* KO	This paper	N/A
Human: HT-1080 *PRDX2* KO	This paper	N/A
Human: HT-1080 *PRDX3* KO	This paper	N/A
Human: HT-1080 *PRDX4* KO	This paper	N/A
Human: HT-1080 *PRDX5* KO	This paper	N/A
Human: HT-1080 *PRDX6* KO + hPRDX6 OE	This paper	N/A
Human: HT-1080 *PRDX6* KO + HA-hPRDX6 OE	This paper	N/A

(*Continued on next page*)

Please cite this article in press as: Ito et al., PRDX6 dictates ferroptosis sensitivity by directing cellular selenium utilization, Molecular Cell (2024), https://doi.org/10.1016/j.molcel.2024.10.028

Continued

REAGENT or RESOURCE	SOURCE	IDENTIFIER
Human: 786-O *PRDX6* KO	This paper	N/A
Human: A375 *PRDX6* KO	This paper	N/A
Human: A549 *PRDX6* KO	This paper	N/A
Human: NCI-H460 *PRDX6* KO	This paper	N/A
Human: LOX-IMVI *PRDX6* KO	This paper	N/A
Human: HEC151 *PRDX6* KO	This paper	N/A
4-hydroxytamoxifen inducible *Gpx4* knockout MEFs (Pfa1 cells)	Seiler et al.[31]	N/A
Mouse: Pfa1 *Gpx4* KO	Nakamura et al.[30]	N/A
Mouse: Pfa1 *Gpx4* KO + HA-mPRDX6 OE	This paper	N/A
Mouse: Pfa1 *Gpx4* KO + HA-hFSP1 OE	Nakamura et al.[35]	N/A
Mouse: Pfa1 *Gpx4* KO + HA-hGCH1 OE	This paper	N/A
Mouse: Pfa1 + hPRDX6 OE	This paper	N/A
Mouse: Pfa1 + FSH-hPRDX6 OE	This paper	N/A
Experimental models: Organisms/strains		
BALB/c nude mice (CAnN.Cg-*Foxn1*^{nu}/Crl)	Charles River	N/A
Prdx6 knockout mice (*Prdx6*^{tm1Abf}/Mmjax)	Jackson Laboratory	MMRRC_043402-JAX
Oligonucleotides		
hPRDX6 sg1_GATAGGATGGGGATAGTGTGA	This paper	N/A
hPRDX6 sg2_GCTCTGTGGTGCACACTG	This paper	N/A
hPRDX6 sg3_GACACTGGGGTAAAGTCCCGA	This paper	N/A
hPRDX1 sg1_GAAAGCAATGATCTCCGTG	This paper	N/A
hPRDX2 sg1_GTTGATGGCGCCTTCAAAG	This paper	N/A
hPRDX3 sg1_GCAGTGGCAGAAATGCCCCA	This paper	N/A
hPRDX4 sg1_GTATTACTTACAAATCAAGT	This paper	N/A
hPRDX5 sg1_GCTCCTGGCTGATCCCACTG	This paper	N/A
mPrdx6 sg1_GACACTGGGGTAAAGTCCCGT	This paper	N/A
Software and algorithms		
GraphPad Prism v10	GraphPad Software	https://www.graphpad.com
Analyst v1.7.2	Sciex	https://sciex.com/
SoftMax Pro v7	Molecular devices	https://www.moleculardevices.com/
Image Lab v6.0	Bio rad	https://www.bio-rad.com/
3D Cell Explorer and Eve software v1.8.2	Nanolive	https://www.nanolive.ch/
FlowJo Software v10	FlowJo	https://www.flowjo.com/
ImageJ/Fiji software v1.53	NIH	https://imagej.net/software/fiji/downloads
MaxQuant version 2.5.2.0	MaxPlack Institute for Biochemistry	https://www.maxquant.org/
Skyline version 23.1.0.455	MacCoss Laboratory, University of Washington	https://www.maccosslab.org/
FreeStyle 1.8 SP2	Thermo Fisher Scientific	https://assets.thermofisher.com/TFS-Assets/CMD/manuals/FreeStyle1.8SP2_Install_Instructions.pdf
Pymol 3.0	PyMol	http://www.pymol.org/pymol

EXPERIMENTAL MODEL AND STUDY PARTICIPANT DETAILS

Cells

Murine immortalized 4-hydroxytamoxifen (TAM)-inducible *Gpx4* knockout (KO) fibroblasts (referred to as Pfa1) were reported previously.[31] Genomic *Gpx4* deletion can be achieved by TAM-inducible Cre recombinase using the CreERT2/LoxP system. HT-1080 (CCL-121), 786-O (CRL-1932), A375 (CRL-1619), A549 (CCL-185), HEK293T (CRL-3216) and NCI-H460 (HTB-177) cells were

obtained from ATCC. LOX-IMVI cells were obtained from NCI/NIH. HEC151 cells (JCRB1122-A) were obtained from JCRB Cell Bank. Pfa1, HT-1080, 786-O, A375 and A549 cells were cultured in DMEM high glucose (4.5 g glucose/L) supplemented with 10% fetal bovine serum (FBS), 2 mM L-glutamine, and 1% penicillin/streptomycin. LOXIMVI, H460 and HEC151 cells were cultured in RPMI 1640 GlutaMax supplement medium (Gibco) with 10% FBS and 1% penicillin/streptomycin. For generating stably overexpressing cell lines, appropriate antibiotics (puromycin 1 μg/mL, blasticidin 10 μg/mL or G418 0.5-1 mg/mL) were used. *GPX4* KO HT-1080 and *Gpx4* KO Pfa1 cells were maintained in a medium containing Lip-1 (1 μM) to prevent ferroptosis. All cells were cultured at 37 ℃ with 5% CO_2 and verified to be negative for mycoplasma.

Animals

Male littermate *Prdx6*$^{-/-}$ and *Prdx6*$^{+/+}$ mice aged 5 weeks and female BALB/c nude mice (CAnN.Cg-Foxn1nu/Crl) aged 7 weeks were used. The animal experiment was performed in compliance with the German Animal Welfare Law or the guidelines of Tohoku University. The experimental protocols were approved by the institutional committee on animal experimentation and the government of Upper Bavaria (ROB-55.2-2532.Vet_02-23-11) and the Animal Welfare Committee at Tohoku University (2023AgA-011). Mice were housed in a specific pathogen free facility at constant temperature and humidity under a light cycle of 12 h on/12 h off set from 6 a.m. to 6 p.m.

METHOD DETAILS

Chemicals

Liproxstatin-1 (Lip-1, Selleckchem, S7699), erastin (Merck, 329600), (*1S,3R*)-RSL3 (RSL3, Cayman, 19288), iFSP1 (Cayman, 29483), ML210 (Cayman, 23282), FIN56 (Cayman, 25180), FINO2 (Cayman, 25096), viFSP1 (Vistas-lab, STK626779), L-buthionine sulfoximine (BSO, Sigma-Aldrich, B2515), auranofin (Sigma-Aldrich, A6733), sulfasalazine (Sigma-Aldrich, S0883), 4-hydroxytamoxifen (4-OH TAM, Sigma-Aldrich, H7904), L-selenocystine (Sigma-Aldrich, 545996), sodium selenite (Sigma-Aldrich, S5261), L-selenomethionine (Sigma Aldrich, S3132), L-glutathione reduced (GSH, Sigma Aldrich, G4251), L-glutathione oxidized (GSSG, WAKO, 79-03333) N-ethylmaleimide (NEM, Nacalai Tesque, 15512-11), MJ33 (Cayman, 90001844) and Imidazole ketone erastin (IKE, Selleckchem, S8877) were purchased. icFSP1 was synthesized by Intonation Research Laboratories.

Lentiviral production and transduction

A lentiviral transduction system was used for generating KO and overexpressing cells. A third-generation lentiviral packaging system consisting of transfer plasmids of the interest, pMD2.G (Addgene, 12259) and psPAX2 (Addgene, 12260) were co-lipofected into HEK293T cells using PEI MAX (Polysciences, 24765). Supernatants containing viral particles were harvested at 2 days post-transfection and filtered through a 0.45 μm PVDF filter (Millipore, SLHV033RS) and stored at -80 ℃ until use. Cells were seeded on 12 well plates with lentivirus particles and protamine sulfate (10 μg/mL) to enhance the transduction efficiency. On the next day, the cell culture medium was replaced with fresh medium containing respective selection antibiotics and cultured until non-transduced cells were dead.

Generation of knockout cells

Gpx4 KO Pfa1 cells, *GPX4* KO HT-1080 cells, *GPX4* KO HT-1080 cells overexpressing hGPX4 were made in the previous studies.[30,67] *PRDX6* KO and *PRDX1-5* KO cells were established by lentiviral transduction. The sequences of single guide RNAs (sgRNA) designed to target exons of the genes of interest based on the VBC score (https://vbc-score.org/) are listed in Key Resource Table. The sgRNAs were subcloned into BsmBI-digested lentiCRISPRv2-puro vector (Addgene, 98290). The lentiviral particles were prepared using a third-generation lentiviral packaging system. One day after the transduction of lentiviral particles containing the transfer plasmid of lentiCRISPRv2-puro inserted sgRNA sequences, the cell culture medium was replaced with media containing puromycin (1 μg/ml). After selection for 2-3 days, single-cell clones were isolated by serial dilution and knockout clones were validated by immunoblotting for the establishment of *PRDX6* KO HT-1080 cells and *PRDX6* KO A549 cells. In other cell lines, polyclonal KO cells without single-cell cloning were subjected to the experiments.

Cloning of plasmids for overexpression

A human *PRDX6* cDNA (NM_004905.3) was cloned from the cDNA of HT-1080 cells and followed by cloning in the p442-blast vector furnished with an N-terminal HA tag. To avoid being targeted by CRISPR-Cas9, sgRNA-resistant mutants were created by site-directed mutagenesis using polymerase KOD One (Sigma, KMM-201NV) followed by ligation using in-Fusion cloning enzymes (Takara Bio, 638948). hPRDX6-p442-blast vector with a N-terminal Flag-Strep II-HA tag and that without a tag were also prepared. hPRDX6 mutants (S32A, C47S and C91S) were generated by site-directed mutagenesis. Codon-optimized *Mus musculus* (mouse) PRDX6 (NP_031479.1) *Homo sapiens* (human) GCH1 (NP_000152.1) were synthesized by Twist Bioscience and cloned into the lentivirus plasmid pLV-Neo with an N-terminal HA tag. Human FSP1 (NM_001198696.2) and short form of human GPX4 (NM_001367832.1) cloned into 442-blast were prepared in the previous studies.[35,67]

Preparation of PCOOH-d_9

To obtain 1-palmitoyl-2-linoleoyl-sn-glycero-3-phosphatidylcholine-d_9 (PC-d_9) as a substrate of PCOOH-d_9, 25 mg of 1-palmitoyl-2-linoleoyl-sn-glycero-3-phosphatidylethanolamine (16:0/18:2-PE, Avanti Polar Lipids, 850756) dissolved in methanol containing NaOH (1 N) was incubated with 250 μL of iodomethane-d_3 (Isotec, 176036) for 6 h at 35 °C. After incubation, PC-d_9 was isolated using preparative thin-layer chromatography and purified by solid phase extraction (Silica, Waters, WAT023595). To obtain PCOOH-d_9, PC-d_9 was subjected to photo-oxidation according to a previous study method with slight modifications.[68,69] Briefly, PC-d_9 was dissolved in methanol containing 40 μM rose bengal, and then the sample was placed under the LED light and oxidized for 48 h at 40 °C. After the oxidation step, the sample was subsequently passed through a Sep-Pak NH_2 cartridge (Waters, WAT023610) to remove rose bengal followed by evaporation and dissolving in methanol. Finally, PCOOH-d_9 was isolated from crude oxidized PC-d_9 using semipreparative LC.

Measurement of PCOOH-d_9 and PCOOH using LC-MS/MS

To prepare cell lysate, cells were harvested and lysed by incubation with 0.1% Triton X-100 solution on ice for 30 min. Following centrifugation at 20,000 × g at 4 °C for 40 min, the supernatant was collected and used for PCOOH reduction assay. For the experiment using heat-treated cell lysate, the supernatant was incubated at 95°C for 60 min, centrifuged at 20,000 × g for 40 min at 4°C, and the heated supernatant was collected. For evaluation of PCOOH-d_9 reduction, 2 μL of PCOOH-d_9 (final conc. 10 μM) dissolved in ethanol was added to 198 μL of cell lysate supernatant, then incubated for 1 h at 37 °C. After the incubation, PCOOH-d_9 was extracted from 180 μL of the incubated sample by the Folch method according to a previously published[70,71] and dissolved in 200 μL of methanol. When affinity-purified GPX4 or recombinant human PRDX6 was used for this assay, 4 μL of affinity-purified GPX4 (0.45, 4.5 and 45 nM) or recombinant human PRDX6 (30, 150 and 300 μM) was incubated with 2 μL of PCOOH-d_9 (final conc. 10 μM) dissolved in 0.1% Triton X-100 and 4 μL of GSH (final conc. 1 mM) for 1 h at 37 °C. After incubation, 5 μL of the mixture was sampled by mixing with 495 μL of methanol. The collected methanol samples were subjected to an LC-MS/MS system (QTRAP 7500 tandem mass spectrometer (SCIEX) equipped with an Exion LC system (SCIEX)). Data was analyzed using Analyst v1.7.2 software (Sciex).

The detailed analytical conditions are as follows: a system consisting of a 7500 QTRAP tandem mass spectrometer (SCIEX) equipped with an Exion LC system (SCIEX). The general LC-MS/MS conditions were as follows: entrance potential, 14.0 V; collision energy, 58.0 V; collision cell exit potential, 30.0 V; temperature, 500°C; source, ESI; and ion polarity, positive. PCOOH-d_9 was detected by multiple reaction monitoring (MRM) for the transition of precursor ions to products: (*m/z* 821>541). Chromatographic separation was performed using an Inertsustain AQ-C18 (3 μm, 2.1 x 150 mm; GL Science) at 40°C. The column was eluted with a mobile phase consisting of solvent A (water containing 0.1% formic acid) and solvent B (methanol containing 0.1% formic acid). The flow rate was 0.4 mL/min. The mobile phase gradient profile was as follows: 0–5 min, 90% B; 5–15 min, 90–100% B linear; 10–15 min, 100% B for Figures 1C and S2D, and 0–2 min, 90% B; 2–8 min, 90%–100% B linear; 8–12 min, 100% B for Figures 1B, 1D, 1E, and S2B. A system consisting of a 4000 QTRAP tandem mass spectrometer (SCIEX) equipped with an Exion LC system. The general LC-MS/MS conditions were as follows: entrance potential, 14.0 V; collision energy, 58.0 V; collision cell exit potential, 30.0 V; temperature, 600°C; source, ESI; and ion polarity, positive. PCOOH was detected by MRM for the transition of precursor ions to products: (*m/z* 812>541). Chromatographic separation was performed using an COSMOSIL 5C18-MS-II (5 μm, 2.1 × 150 mm, Nacalai tesque) at 40°C. The column was eluted with a mobile phase consisting of solvent A (water containing 0.1% formic acid) and solvent B (methanol containing 0.1% formic acid). The mobile phase gradient profile was as follows: 0–2 min, 92% B; 2–10 min, 92–98% B linear; 10–14 min, 98–100% B linear; 14–20 min, 100% B. The flow rate was 0.2 mL/min. This condition was used for Figure S2C.

Preparation of affinity-purified GPX4

Affinity-purified GPX4 was collected from *Gpx4* KO Pfa1 cells stably overexpressing N-terminal Flag-Strep II-HA-tagged hGPX4 as reported previously with minor modifications.[30] Briefly, the cells were treated with sodium selenite (200 nM for 2 day), harvested, lysed in LCW lysis buffer (0.5% Triton X-100, 0.5% sodium deoxycholate salt, 150 mM NaCl, 20 mM Tris-HCl, 10 mM EDTA and 30 mM sodium pyrophosphate tetrabasic decahydrate, pH 7.5) and supernatant was collected after centrifugation at 20,000 g for 30 min at 4°C. Tagged GPX4 was affinity-purified from the supernatant by incubation with MagStrep XT beads (IBA Lifesciences) for 1 h at 4°C on a rotator. The beads were washed three times with washing buffer (100 mM Tris-HCl pH 8, 150 mM NaCl and 1 mM EDTA) followed by elution using the elution buffer (100 mM Tris-HCl pH 8, 150 mM NaCl, 1 mM EDTA and 50 mM biotin). Protein concentration was determined by silver staining of SDS-PAGE gel using bovine serum albumin as a concentration standard.

Measurement of PCOOH in the mouse liver by LC-MS/MS

Frozen-stored tissues collected from *Alb-creERT2; Gpx4$^{fl/fl}$* (hepatocyte-specific *Gpx4* KO) and *Cre(-); Gpx4$^{fl/fl}$* control mice (equal distribution of sex and weight, aged 8–10 weeks) fed a low vitamin E diet (containing <7 mg/kg vitamin E, E15314-247, ssniff Spezialdiäten) for seven days after tamoxifen injection (2 mg on two consecutive days, dissolved in Miglyol 812, Caelo) were used. These tissues were the samples collected from the same mice used in the previous study[14] and stored at -80°C. All experiments were performed in compliance with the German Animal Welfare Law and have been approved by the institutional committee on animal experimentation and the government of Upper Bavaria (approved no. ROB-55.2-2532-Vet_02-18-13). Total lipids containing

PCOOH were extracted from the mouse liver samples by the Folch method.[71,72] PCOOH was analyzed using LC-MS/MS system (QTRAP 6500+ tandem mass spectrometer (SCIEX) equipped with an Exion LC system (SCIEX)) as described previously.[73–75] Data was analyzed using Analyst v1.7.2 software (Sciex).

Cell viability assay

Cells were seeded on 96-well plates and cultured overnight (2×10^3 cells/well for ferroptosis inducer treatment except for BSO and 4-OH TAM and 500 cells/well for BSO and 4-OH TAM treatment). The next day, the medium was replaced with medium containing the compounds described in the corresponding figure legends at the indicated concentrations. After incubation for 24 h (RSL3, ML210, FIN56, FINO2 and auranofin), 48 h (erastin and sulfasalazine) and 72 h (BSO, iFSP1, viFSP1, icFSP1 and 4-OH TAM), the culture medium was replaced with medium containing 0.004% resazurin to access cell viability. Fluorescence was measured at Ex/Em = 540/590 nm using a SpectraMax M5 microplate reader or Spectra Max iD5 (Molecular devices) with SoftMax Pro v7 (Molecular devices) after 4 h of incubation in the medium containing resazurin.

Deprivation and supplementation of selenium

For selenium deprivation, cells were incubated with selenium-free (Se-free) medium (DMEM high glucose medium containing 2.5 mg/mL bovine serum albumin, 5 μg/mL insulin, 5 μg/mL transferrin, 92 nM $FeCl_3$, 2 mM L-glutamine and 1% penicillin-streptomycin.[76] For the immunoblotting assay, cells were harvested after incubation with Se-free medium supplemented Lip-1 (0.5 μM; to prevent ferroptosis) for 48-72 h. Cell viability was measured 24 h after replacing with Se-free media. For supplementation with L-selenocystine, sodium selenite or Lip-1, these were added to the Se-free medium at the timing of medium replacement.

Cyst(e)ine and GSH deprivation

For cyst(e)ine (Cys) deprivation, cells were incubated with cystine/methionine-free high glucose DMEM (Gibco, 21013024) supplemented with 10% dialyzed FBS (Thermo Fisher, A3382001), 100 μM methionine, 1 mM sodium pyruvate, 2 mM L-glutamine and 1% penicillin-streptomycin. For the immunoblotting assay, cells were harvested 48-72 h after incubation in the Cys-free medium supplemented Lip-1 (0.5 μM, to prevent ferroptosis induced by Cys deprivation) or β-mercaptoethanol (β-ME, 50 μM). For BSO and/or erastin treatment, cells were harvested after incubation with normal culture media containing BSO (500 μM) and/or erastin (10 μM) with Lip-1 (0.5 μM; to prevent ferroptosis). L-selenocystine, sodium selenite and selenomethionine were added at the same time when the medium was replaced unless specifically stated otherwise.

LDH release assay

HT-1080 cells (2×10^3 cells/well) were seeded on 96-well plates and cultured overnight. On the next day, the medium was changed to a selenium deprivation medium. Released LDH was assessed using the Cytotoxicity Detection kit (Roche, 11644793001) to determine cell death. In brief, cell culture supernatant was collected as a medium sample; then cells were lysed using 100 μL of 0.1% Triton X-100 in PBS as a lysate sample. Medium and lysate samples were individually loaded with reagents onto microplates, and the absorbance was measured at 492 nm using a SpectraMax M5 microplate reader after 15 min incubation at room temperature. LDH release (%) was calculated using medium sample values divided by the sum of medium and lysate sample values.

Immunoblotting

Cells were lysed in LCW lysis buffer (0.5% Triton X-100, 0.5% sodium deoxycholate salt, 150 mM NaCl, 20 mM Tris-HCl, 10 mM EDTA and 30 mM sodium pyrophosphate tetrabasic decahydrate, pH 7.5) containing protease and phosphatase inhibitor mixture (cOmplete and phoSTOP; Roche, 04693116001 and 4906837001) and centrifuged at 20,000 × g for 40 min at 4 °C. After addition of 6 × SDS sample buffer (375 mM Tris-HCl, pH 6.8, 9% SDS, 50% glycerol, 9% β-mercaptoethanol and 0.03% bromophenol blue) to the collected supernatant and heating at 55 ℃ for 3 min, the samples were resolved on 12% SDS-PAGE gels and electroblotted onto a PVDF membrane (Bio-Rad, 170-4156). The membrane was blocked with 5% skim milk (Carl Roth, T145.2) in TBS-T (20 mM Tris-HCl, 150 mM NaCl and 0.1% Tween-20) and then probed with the primary antibodies against GPX4 (1:1,000, ab125066, Abcam), GPX1 (1:1,000, ab22604, Abcam), PRDX6 (1:1,000, 95336S, Cell Signaling Technology), PRDX1 (1:1000, rabbit, kindly provided by Dr. Christopher Horst Lillig, Greifswald, Düsseldorf),[65] PRDX2 (1:1000, rabbit, provided by Christopher Horst Lillig, Greifswald, Düsseldorf),[66] PRDX3 (1:1,000, Abcam, ab129206), PRDX4 (1:1,000, ab184167, Abcam), PRDX5 (1:1,000, ab180587, Abcam), FSP1 (1:1000, Santa Cruz, sc-377120), SELENOT (1:500, HPA039780, Sigma Aldrich), SELENOS (1:500, HPA010025, Sigma Aldrich), SEPHS2 (1:500, 14109-1-AP, Proteintech), TXNRD1 (1:1000, ab124954, Abcam), TXNRD2 (1:1000, ab180493, Abcam), HA (1:1,000, clone 3F10, rat IgG1, developed in-house), valosin containing protein (VCP, 1:10,000, ab11433, Abcam) and β-actin-HRP (1:5,000, A3854, Sigma Aldrich). Images were analyzed with Image Lab 6.0 software (Bio-Rad).

Live-cell imaging

HT-1080 cells (6×10^4 cells/well) were seeded on μ-Dish 35 mm low (80136, i-bidi) and incubated overnight. On the next day, live-cell imaging was performed using 3D Cell Explorer and Eve software v1.8.2 (Nanolive). During imaging, the cells were maintained at 37 °C and 5% CO_2 by using a temperature-controlled incubation chamber.

Please cite this article in press as: Ito et al., PRDX6 dictates ferroptosis sensitivity by directing cellular selenium utilization, Molecular Cell (2024), https://doi.org/10.1016/j.molcel.2024.10.028

Lipid peroxidation assay

HT-1080 cells (1 × 10^5 cells/well) were seeded on 12-well plates one day before the experiments. On the next day, the cell culture medium was replaced with selenium deprivation media for 180 min and subsequently incubated with C11-BODIPY 581/591 (1.5 μM, Invitrogen, D3861) for 30 min in a 5% CO_2 atmosphere at 37°C. The cells were washed with PBS, trypsinized and resuspended in 500 μL PBS. After passing through a 40 μm cell strainer, cells were analyzed on a flow cytometer (CytoFLEX, Beckman Coulter) equipped with a 488 nm laser for excitation. Data was collected using CytExpert v2.4 (Beckman Coulter) from the FITC detector (oxidized BODIPY) with a 525/40 nm bandpass filter. At least 10,000 events were analyzed per sample. Data was analyzed using FlowJo Software (v10, FlowJo LLC).

Database analysis

Proteomics data and CRISPR co-dependency of PRDX6 were minded from depmap (http://www.depmap.org; version v23Q4). Co-essentiality analysis was performed using Co-essentiality browser (http://coessentiality.net/; date obtained in 2024.01).

qPCR analysis

Total RNA was extracted from cells with RNeasy Mini kit (Qiagen, 74104) and followed by genomic DNA digestion using RNase-free DNase (Qiagen, 79254). cDNA was synthesized by QuantiTect Reverse Transcription Kit (Qiagen, 5001473). Quantitative RT-PCR (qPCR) was carried out by PowerUp SYBR Green Master Mix (Thermo Fisher, A25778) using qTOWER3 G (Analytikjena). All samples were performed with technical triplicates with the following PCR condition: [1] 50℃ for 2 min; [2] 95℃ for 2 min; [3] 95℃ for 15 sec; [4] 59.5℃ for 15 sec; [5] 72C for 1 min; [6] 95C 1 sec - cycle from 3 to 5 was repeated 40 times. Sequences of the primers were the following: 5'- TGCTCTGTGGGGCTCTG -3' and 5'- ATGTCCTTGGCGGAAAACTC -3' for short form GPX4; and 5'-GGTGTGAAC CATGAGAAGTATGA -3' and: 5'-GAGTCCTTCCACGATACCAAAG-3' for GAPDH. The relative GPX4 expression was normalized to GAPDH by the ΔΔCT method.

Measurement of cellular selenium level

To measure total cellular selenium levels, WT and *PRDX6* KO HT-1080 cells (2 × 10^5 cells per well) were seeded on 6-well plates with standard culture medium. The following day, the medium was replaced with either standard culture medium containing Lip-1 (1 μM) or cyst(e)ine-free medium containing Lip-1 (1 μM) with or without supplementation of L-selenocystine (100 nM) or sodium selenite (100 nM). After 24 h of incubation, the cells were washed with PBS and harvested in 200 μL of PBS. The cells were separated into two aliquots and collected by centrifugation (1,000 × g, 3 min, 4℃). One aliquot was solubilized with 1% SDS to determine protein content and the other aliquot was mixed with 1 mL 30% HNO_3 and subjected to ICP-MS 8900 (Agilent). Data was normalized by the corresponding protein concentration.

Structural data of PRDX6

The structure of the dimerized human PRDX6 (PDB: 5B6M) was displayed using pymol 3.0 (http://www.pymol.org/pymol) for highlighting key functional residues

Preparation of recombinant PRDX6 protein

Recombinant hPRDX6 was purified as published previously.[77] In summary, codon-optimized human PRDX6 gene (UniProt P30041) was ordered as linearized DNA (Integrated DNA Technologies) and cloned into a petM11 vector containing a N-terminal cleavable 6-histidine tag and transformed into BL21 cells. One L of cells were grown in TB media and expression was induced by IPTG when the cells reached OD600 of 2.0 and the temperature was kept at 20°C during 16 h. After harvesting, cells were dissolved in lysis buffer containing 20 mM HEPES 7.5, 200 mM NaCl, 5% glycerol, 10 mM imidazole and 1 mM β-ME and subjected to sonication. The soluble part was obtained by centrifugation at 35,000 × g and the supernatant was applied onto a nickel resin. After extensive wash, the protein was eluted with a lysis buffer supplemented with 350 mM imidazole. The N terminal 6-histidine tag was cleaved overnight by TEV protease and at the same time the protein was dialyzed into lysis buffer. Non-tagged PRDX6 was purified using a nickel column, where the flow through was collected, concentrated and applied to the final purification step, size exclusion chromatography, using a S200 high load column pre-equilibrated with 10 mM HEPES pH 7.5, 100 mM NaCl. The identity of the protein was confirmed by running a denaturing SDS gel. The protein was flash frozen in liquid nitrogen and stored at -80°C until further usage.

MS analysis of PRDX6-selenium adducts

For detection of PDRX6-selenium adducts, 100 μM recombinant hPRDX6 was incubated for 10 min at room temperature with 100 μM sodium selenite, 300 μM GSH and 50 mM HEPES pH 7 in water. In control experiments, either sodium selenite or GSH was omitted from the reaction. Subsequently, iodoacetamide was added to a final concentration of 10 mM from a 100 mM aqueous stock solution and the mixture incubated for 10 min at 37°C. Five μg of PRDX6 was subsequently digested with 0.33 μg trypsin in 40 mM HEPES pH 7 for 3 h at 37°C and resulting peptides desalted by solid phase extraction using an Oasis PRiME HLB 96-well μElution plate (Waters) according to the manufacturer's instructions. One-hundred ng of peptides were subsequently analyzed by LC-MS (UltiMate 3000 rapid separation liquid chromatography system (Thermo Fisher Scientific) as described earlier with minor modifications.[78] Data

was analyzed with MaxQuant version 2.5.2.0 (MaxPlack Institute for Biochemistry) and Skyline version 23.1.0.455 (MacCoss Laboratory, University of Washington).

The detailed analytical conditions are as follows: after stacking on a 2 cm C18 pre-column, peptides were separated over one hour on an aurora ultimate C18 column (25 cm, 75 μm inner diameter, 1.7 μm bead size, IonOptics) using an UltiMate 3000 rapid separation liquid chromatography system (Thermo Fisher Scientific). Subsequently, peptides were injected via a nano-source electrospray interface into a QExactive plus (Thermo Fisher Scientific) quadrupole-Orbitrap mass spectrometer operated in data-dependent positive mode. After recording of a precursor spectrum (resolution 140000, automatic gain control target 3000000, maximum ion time 50 ms, scan range 200–2000 *m/z*, profile mode), up to 20 precursors with charge states +2 and +3 were selected by the build-in quadrupole (4 *m/z* isolation window), fragmented by higher-energy collisional dissociation (normalized collision energy: 30) and fragment spectra recorded in the Orbitrap analyzer (resolution 17500, automatic gain control target 100000, maximum ion time 50 ms, scan range 200–2000 *m/z*, centroid mode). Dynamic exclusion was set to 10 seconds. Resulting spectra were analyzed by MaxQuant version 2.5.2.0 (MaxPlack Institute for Biochemistry) using an amino-acid sequence from PRDX6 and potential contaminants included in MaxQuant. Following variable modifications were included in the search: methionine oxidation, protein-N-terminal acetylation, cysteine sulfinic acid, cysteine sulfonic acid, glutathionylation at cysteine, cysteine carbamidomethylation. Disulfides were included as crosslinks and a search for dependent peptides enabled. Precursor intensities of cysteine containing peptide species including the above-mentioned variable modification as well as Se + carbamidomethyl (monoisotopic peak +136.938) and Se + glutathione (monoisotopic peak +384.9847) was quantified with Skyline version 23.1.0.455 (MacCoss Laboratory, University of Washington). Retention times were mapped on the basis of MaxQuant search results, extracted ion chromatograms (FreeStyle 1.8 SP2, Thermo Fisher Scientific) and characteristic Se isotope patterns in precursor spectra.

Synthesis of GS-Se-SG

(2*S*,7*R*,13*R*,18*S*)-2,18-diamino-7,13-bis((carboxymethyl)carbamoyl)-5,15-dioxo-9,11-dithia-10-selena-6,14-diazanonadecanedioic acid (GS-Se-SG) was synthesizes based on the previous report.[79] In a two-necked flask was placed selenium dioxide (16.6 mg, 0.15 mmol) in H_2O (1.0 mL) under an argon atmosphere, and the solution was stirred at 0 °C. Then the solution of glutathione reduced (230.5 mg, 0.75 mmol) in H_2O (1.5 mL) was added dropwise, and the mixture stirred at 0 °C for 1 h. The precipitated solid was collected by filtration and washed with cold water. The solid was dried under reduced pressure giving (2*S*,7*R*,13*R*,18*S*)-2,18-diamino-7,13-bis((carboxymethyl)carbamoyl)-5,15-dioxo-9,11-dithia-10-selena-6,14-diazanonadecanedioic acid (52.6 mg, 51%).

Detection of selenium binding to PRDX6 by ICP-MS

Recombinant hPRDX6 was prepared using human PRDX6 expression vector cloned into pET21b (kindly provided by Dr. Aron B. Fisher, University of Pennsylvania) as reported previously.[80] Purified PRDX6 protein was concentrated and desalted by ultrafiltration (Amicon ultra centrifugal filter, 10 kDa MWCO, Merck), replaced with PBS, frozen in liquid nitrogen, and stored at -80°C until before use. The purity of recombinant PRDX6 was confirmed by Coomassie Brilliant Blue staining followed by SDS-PAGE and was greater than 99%. Site-directed mutation of C47S was performed by KOD plus Mutagenesis Kit (TOYOBO) with primers 5'- AGCAC CACAGAGCTTGGCAG-3' and 5'- CACTGGGGTAAAGTCCCGAG-3' according to manufacturer's instruction. Recombinant PRDX6 protein (40 μM) was reacted with sodium selenite (40 μM) and GSH (160 μM) or GS-Se-SG (40 μM) in PBS for 10 min at 37°C. The mixture was then prepared to 100 μL by water, and 400 μL of methanol was added and mixed. Then 100 μL of chloroform was added and mixed, followed by 300 μL of water. After centrifugation (15,000 × g for 2 min at 4°C), the resulting precipitate was washed twice with 400 μL of methanol to remove excess reagents. To the air-dried precipitate, 1 mL of 30% HNO_3 was added and ICP-MS analysis was performed by Agilent 8900 (Agilent).

Prdx6 deficient mice

Frozen-thawed sperm from *Prdx6* knockout mice[55] (*Prdx6*^{tm1Abf}/Mmjax, MMRRC_043402-JAX, obtained from the Jackson Laboratory) were used for in vitro fertilization and transplanted into female C57BL/6J recipient mice to obtain heterozygous *Prdx6* knockout mice. Homozygous *Prdx6* knockout (*Prdx6*$^{-/-}$) mice and *Prdx6* wild-type (*Prdx6*$^{+/+}$) mice were generated by intercrossing the heterozygous mice. The following primers were used for genotyping PCR: WT forward, 5'-TGTGATGGTGGTTCCTTGG; KO forward: 5'-AGACTGCCTTGGGAAAAGCG; and common reverse, 5'-TGGCTCAAGCATTCACACAG (WT = 289 bp, KO = ∼200 bp). At five weeks of age, male littermate *Prdx6*$^{-/-}$ and *Prdx6*$^{+/+}$ mice fed a normal diet (CE-2, CLEA Japan) were euthanized. The whole brain, liver and kidney were collected from these mice and used for immunoblotting analysis.

Xenograft subcutaneous tumor experiments

Female BALB/c nude mice (CAnN.Cg-Foxn1nu/Crl, Charles River) aged 7 weeks were randomly divided into four groups. Wild-type A549 cells expressing Cas9 or *PRDX6* KO A549 cells (4 × 10^6 cells in 100 μL PBS) were subcutaneously injected into the backs of the mice. Starting four days post-inoculation, the mice were treated with either IKE (40 mg/kg/day dissolved in 60% PEG-400, 10% Tween-80 and 30% D5W (5% dextrose in water) or vehicle via daily intraperitoneal injection. Twenty-five days post-treatment, the mice were euthanized and tumors were collected.

Please cite this article in press as: Ito et al., PRDX6 dictates ferroptosis sensitivity by directing cellular selenium utilization, Molecular Cell (2024), https://doi.org/10.1016/j.molcel.2024.10.028

QUANTIFICATION AND STATISTICAL ANALYSIS

Statistical analysis

Statistical information for individual experiments can be found in the corresponding figure legends. Graphs were created using GraphPad Prism v10 (GraphPad Software).